Revision 1

Analysis of hydrogen and fluorine in pyroxenes: Part II. Clinopyroxene

JED L. MOSENFELDER[1]* and GEORGE R. ROSSMAN[1]

[1]Division of Geological and Planetary Sciences, California Institute of Technology, M/C 170-25, Pasadena, California 91125-2500, U.S.A.

*E-mail: jed@gps.caltech.edu

ABSTRACT

We measured hydrogen in 13 natural clinopyroxenes using Fourier transform infrared (FTIR) spectroscopy. $^{16}O^{1}H/^{30}Si$ and $^{19}F/^{30}Si$ were also measured in the samples using secondary ion mass spectrometry (SIMS). H data were compared between the two techniques and F was calculated with reference to F-bearing silicate glass standards. Four of the clinopyroxenes are used as standards for SIMS calibration in multiple laboratories, and three have been measured previously using hydrogen manometry and/or elastic recoil detection analysis. Compared to clinopyroxenes in previous surveys comparing FTIR and SIMS, the 13 samples cover a broader range in chemistry and band positions in the O-H vibrational spectrum. They also all lack detectable amphibole lamellae, which are otherwise commonly present in this mineral group. In contrast to orthopyroxene, the SIMS and FTIR data for clinopyroxene show significantly better correlations (r^2 = 0.96-0.98) when the frequency-dependent IR calibration of Libowitzky and Rossman (1997) is applied, as opposed to the Bell et al. calibration (r^2 = 0.92-93). We derive a frequency-dependent molar absorption coefficient with parameters different from those of Libowitzky and Rossman's calibration, which was established using data on stoichiometric hydrous phases and gives poor agreement with the manometrically determined value for PMR-53. Comparison of data for PMR-53 to our SIMS calibrations for orthopyroxene and olivine suggests that the matrix effect among these phases is less than 20% relative. Fluorine concentrations vary depending on geological context, with the highest concentrations (up to 214 ppm) found in diopsides from crustal metamorphic environments. Mantle samples follow similar geographic trends as olivines and orthopyroxenes, with higher F in xenocrysts from Kilbourne Hole (46 ppm) and South African kimberlites (up to 29 ppm) compared to the Colorado Plateau (8 ppm). On the basis of chemical correlations, we propose two different incorporation mechanisms for F:

1) coupled subsititution with Al^{3+} and/or Fe^{3+} in tetrahedral sites; and 2) coupled substitution with monovalent cations (Na and K) in the M2 site. The second substitution is more relevant to mantle augites than crustal diopsides. The F concentrations we measured are much lower than those in some clinopyroxenes synthesized in recent high P-T studies. Nevertheless, our data support suggestions that the F budget of the mantle can be entirely accommodated by incorporation in nominally anhydrous/fluorine-free minerals.

Keywords: FTIR, SIMS, mantle, calibration, nominally anhydrous minerals

INTRODUCTION

In part I of this study (Mosenfelder and Rossman in press) we assessed the quantitative aspects of measuring trace amounts of hydrogen and fluorine in orthopyroxene using two complimentary techniques, Fourier-transform infrared spectroscopy (FTIR) and secondary ion mass spectrometry (SIMS). Here we employ the same approach for clinopyroxene. Studies of mantle samples (Bell and Rossman 1992; Ingrin and Skogby 2000; Peslier et al. 2002; Bell et al. 2004; Grant et al. 2007; Li et al. 2008; Sundvall and Stalder 2011) consistently show that clinopyroxene has the highest H contents among co-existing, volumetrically important nominally anhydrous minerals (NAMs). Consequently, clinopyroxene should exert a strong influence on processes such as mineral-melt H partitioning, in accord with experimental studies (Aubaud et al. 2004, 2008; Hauri et al. 2006; Tenner et al. 2009; O'Leary et al. 2010). Significant amounts of H have also been measured in clinopyroxenes from crustal sources, such as metamorphic diopsides (Johnson et al. 2002) and phenocrysts from arc volcanic rocks (Wade et al. 2008; Nazzareni et al. 2011). Less is known about F in clinopyroxene, but a recent experimental study (Dalou et al.

2012) measured up to ~600 ppm F in clinopyroxenes formed in equilibrium with basaltic melts at high pressure and explored possible structural mechanisms for incorporation of this element.

Accurate quantification of hydrogen in clinopyroxene is clearly a desirable goal, yet significant challenges remain. Polarized FTIR spectroscopy requires careful sample orientation, which is inherently more difficult for monoclinic pyroxenes compared to minerals with higher symmetry such as olivine, orthopyroxene, and garnet. Unpolarized FTIR spectroscopy (Katayama et al. 2006; Kovács et al. 2008) is much more convenient, but subject to large uncertainties (Withers, in press), especially considering the exceptional degree of anisotropy in band structures in the O-H vibrational region that clinopyroxene can exhibit (e.g., Johnson et al. 2002). Large variations in band positions have also prompted concern (Bell et al. 1995; Ingrin and Skogby 2000) that a frequency-dependent calibration might be more appropriate for clinopyroxenes, rather than the single molar absorption coefficient measured by Bell et al. (1995) on a mantle-derived augite using manometry; consequently, many studies (e.g., Stalder and Ludwig 2007; Nazzareni et al. 2011) prefer the calibration of Libowitzky and Rossman (1997). It must be noted that Libowitzky and Rossman's equation was derived from data on stoichiometric, hydrous minerals, and therefore that its application to rigorous quantification of trace amounts of H in NAMs needs to be verified; in fact, for several NAMs, their calibration (or the similar frequency-dependent relationship derived by Paterson 1982) has been shown to be highly inadequate (e.g., Bell et al. 1995, 2003; Koch-Müller and Rhede 2010). A final issue to consider for FTIR is accuracy in baseline correction, which suffers from similar uncertainties as orthopyroxene (Bell et al. 1995, 2004; Mosenfelder and Rossman in press).

For all of the reasons above as well as other inherent advantages such as enhanced spatial resolution and rapidity of data throughput, SIMS is becoming a technique of choice for

83 measuring H; it is also a convenient and powerful method for simultaneously measuring F and
84 other elements of interest. However, published SIMS calibrations for H in clinopyroxene usually
85 show more data scatter than for other NAMs (Aubaud et al. 2007; Wade et al. 2008; Tenner et al.
86 2009; O'Leary et al. 2010), possibly tied to uncertainties propagated from FTIR. We approached
87 this problem by conducting a combined polarized FTIR and SIMS study on a suite of 13 natural
88 clinopyroxenes, including the primary manometry standard PMR-53 from Bell et al. (1995) as
89 well as three other secondary standards from Bell et al. (2004) (ROM271-DI10, ROM271-DI16
90 and ROM271-DI21) that along with PMR-53 are routinely used for calibration in other ion
91 microprobe laboratories (Carnegie Institute of Washington and Arizona State University) and/or
92 have been studied by Aubaud et al. (2009) using elastic recoil detection analysis (ERDA).
93 Overall, our sample suite spans a wider range in chemistry and IR band structures compared to
94 the study of Aubaud et al. (2007) (see also Tenner et al. 2009), who also offered a
95 comprehensive comparison between SIMS and FTIR data.
96
97 **ANALYTICAL METHODS**
98 Our analytical methods are largely discussed in part I (Mosenfelder and Rossman in
99 press) and in Mosenfelder et al. (2011); additional details follow.
100
101 **Sample preparation and FTIR**
102 For most clinopyroxenes we employed either a McCrone detent spindle stage or Supper spindle
103 stage (Gunter 2004) to orient sections for FTIR. In addition to the newly studied samples listed
104 in Table 1, we oriented additional crystal fragments for some samples studied previously (Bell et
105 al. 1995, 2004; Bell and Ihinger 2000). When possible we made cuboids (single crystals with two

or three orthogonal sets of parallel polished faces) sufficiently large enough to measure all three principal optical directions (α, β, and γ, where β || [010]); some samples required preparation of two separate plates to obtain all three spectra. We did not collect spectra in the **E** || [001] direction for all samples, because we are interested here in quantification based on total integrated absorbance ($\sum A_\alpha + A_\beta + A_\gamma$) and not a full determination of the polarization of individual absorption bands as described by Dowty (1978). We estimate the accuracy of crystal orientations to be ±5° or better. Higher accuracy (±1°) is estimated for diopside 62047-70B, which was originally oriented by X-ray diffraction (Shannon et al. 1992). Band structures in the Si-O overtone region were used to confirm polarization directions, and for this purpose we used well-oriented crystals of 62047-70B and PMR-53 (Bell et al. 1995) as our "reference standards" for diopside and augite, respectively (Fig. 1). Some intermediate compositions, such as ROM271-DI10 (a high calcium number augite), show patterns intermediate between those of 62047-70B and PMR-53, but the diopsides (CIT17210, BPcpxA, 62047-70B, FRB118, JLM77, and 95ADK1A) showed little variation in this spectral region.

Sample densities (Table 1) were determined via Archimedes' method using immersion in toluene. For crystals that were too small to measure accurately with our balance, we made the following assumptions: 1) for diopsides with less than ~2.2 wt% FeO, we used the measured value (3.295 Mg/m^3) for 62047-70B; 2) for augites, we used the measured value (3.339 Mg/m^3) for PMR-53 (Bell et al. 1995), which was reproduced while measuring the densities of other samples here; and 3) for omphacite HRV-147, we used the average calculated value (3.34 Mg/m^3) from McCormick (1987), who conducted a detailed X-ray and chemical study on a suite of omphacites from mantle xenoliths (including five from the same locality as HRV-147). The

contribution of uncertainties in density to overall uncertainties in H concentrations is on the order of 0.5%.

Hydrogen concentrations (given in Table 1 as ppmw H_2O) were calculated from FTIR spectra using a modified form of the Beer-Lambert law ($A = \varepsilon_i \times$ path length × concentration, where ε_i is the integral molar absorption coefficient), applying the three different calibrations of Bell et al. (1995), Aubaud et al. (2009), and Libowitzky and Rossman (1997). Values for ε_i for these three calibrations are 38,300±1700 l mol$^{-1}_{H2O}$ cm^{-2}, 46,103±5300 l mol$^{-1}_{H2O}$ cm^{-2}, and 246.6 • [3753-ν], respectively, where ν in the last case is wavenumber in cm^{-1}. For omphacite HRV-147, we also calculated alternative concentrations using two other values for ε_i published in the literature: 1) 65,000 l mol$^{-1}_{H2O}$ cm^{-2}, the average value derived by Koch-Müller et al. (2007) from SIMS and polarized FTIR measurements of three well-oriented omphacites; and 2) 83,400 l mol$^{-1}_{H2O}$ cm^{-2}, estimated by Katayama et al. (2006) from SIMS and unpolarized FTIR measurements on six omphacites. The accuracy of these determinations is discussed below.

FTIR spectra in the O-H vibrational region (from about 3000-3750 cm^{-1}) were first baseline corrected by manually applying spline fits using the built-in routine in Nicolet's OMNIC software; our baselines and corrected spectra are provided in the supplementary material. Uncertainties in this correction were assessed individually for each of the three spectra used to calculate total absorbance, as reflected in Table 1; they range from 1% to 15% depending on a variety of factors (primarily the height and position of the anisotropic Fe^{2+} absorption band near 4300 cm^{-1}, which largely controls the slope of the baseline, but also other factors such as spectral noise and interference of O-H vibrations with Si-O second overtones). Final uncertainties for H concentrations calculated using the Bell et al. (1995) calibration were estimated by propagating these subjective error estimates with the 2σ uncertainty in the absorption coefficient (8.9%

relative) and the uncertainties in density (which were inconsequential when propagated), while ignoring uncertainties in thickness and possible misorientation of the crystal sections. The resulting relative uncertainties range from 9 to 11.5%, in good accord with the blanket estimation of 10% uncertainty used by Bell et al. (2004). We assumed the same relative uncertainties for H concentrations measured using the Libowitzky and Rossman (1997) calibration, and conducted a similar error propagation exercise for the Aubaud et al. (2009) calibration (in this case using stated uncertainties and values for the three samples that were measured by ERDA in that study).

SIMS

SIMS data [see Mosenfelder et al. (2011) and Mosenfelder and Rossman (in press) for methods] are summarized in Table 2 and provided in unabbreviated form in the supplementary material. Blank correction was performed using measured $^{16}O^{1}H/^{30}Si$ and $^{19}F/^{30}Si$ ratios in GRR510, a V-rich diopside grown from a melt by Jun Ito using a KVO_3 flux and slow cooling from 1350 to 800 °C (Ito, pers. comm.; see Ito (1975) for general methods). No H was detected in this sample using FTIR, and its low measured ^{19}F counts are comparable to those measured for the other nominally blank standards – GRR1017 forsterite and GRR247 enstatite – used in Mosenfelder and Rossman (in press), as well as synthetic zircon (unpublished data). Slightly elevated $^{16}O^{1}H/^{30}Si$ ratios measured for a laboratory-dehydrated clinopyroxene [ZM1cpx-HT; for methods, see Mosenfelder and Rossman (in press)] suggest that this alternative "blank standard" did not completely dehydrate, so it was not used for correction. The uncorrected $^{16}O^{1}H/^{30}Si$ and $^{19}F/^{30}Si$ ratios for GRR510 dropped from 6.1×10^{-4} to 3.1×10^{-4} and 9.7×10^{-4} to 6.8×10^{-4}, respectively, as the blank improved during the session. Detection limits for H and F are given in

Mosenfelder and Rossman (in press) and are well below measured values for all non-blank samples.

Electron probe microanalysis (EPMA)

EPMA data [see Mosenfelder and Rossman (in press) and papers cited therein for analytical details] are given in Table 3. Vanadium was assumed to be only trivalent except in GRR510, for which unpublished optical spectra indicate the predominance of the oxovanadium complex VO^{2+} (this molecular species results in a bright blue color, whereas the V^{3+}-rich natural diopsides exhibit yellowish green colors, as described by Fritz et al. 2007). Cation proportions were calculated on a four-cation basis, with Fe^{3+} estimated using the method of Droop (1986). This procedure, as opposed to normalization to six oxygens, ignores the presence of cation vacancies (known to be particularly prevalent in HRV-147, for which an alternative analysis is given by Smyth et al. 1991) and is of course a much less accurate method for determining Fe^{3+}/Fe^{2+} ratios than techniques such as Mössbauer spectroscopy. For the sake of Table 3 we also ignore the trace components H and F.

RESULTS

IR spectroscopy

FTIR spectra in the three optical directions (α, β and γ) for all samples (except GRR510 and ZM1cpxHT, which show no absorbance in the O-H region) are shown in Figures 2-4. Unlike some of the orthopyroxenes we measured (Mosenfelder and Rossman in press), none of the clinopyroxenes show any evidence for amphibole lamellae (i.e., no bands near 3675 cm^{-1}), which are otherwise commonly seen in this mineral group (Skogby et al. 1990). We also found no

196 significant OH zoning in any of the samples, and no evidence for other hydrous inclusions as
197 documented by Koch-Müller et al. (2004) in some omphacites.

198 In line with previous studies (Skogby et al. 1990; Johnson et al. 2002; Bell et al. 2004),
199 spectra of diopsides (Fig. 2) are much more variable than spectra of augites (Fig. 3). The
200 pleochroism of the bands follows the scheme outlined by Skogby et al. (1990): high wavenumber
201 bands (centered at 3645 cm^{-1} in diopside and between ~3620-3635 cm^{-1} in augite) show
202 absorbance in the order $\alpha \approx \beta >> \gamma$ while lower wavenumber bands (between about 3300 and
203 3550 cm^{-1}) follow the reverse order ($\gamma > \alpha \approx \beta$), as exemplified by the strong bands in Figure 2c
204 for JLM77 and the band at 3470 cm^{-1} in omphacite (Fig. 4). Figure 4 highlights the difference
205 between the Bell et al. (1995) and Libowitzky and Rossman (1997) IR calibrations. The augite
206 and omphacite samples that are compared have similar total absorbance and thus H_2O
207 concentration according to the Bell et al. calibration (552 for augite KBH-2 vs. 565 ppm for
208 omphacite HRV-147). When the frequency-dependent calibration is applied, however, the lower
209 mean wavenumber for HRV-147 results in a much larger discrepancy in calculated H contents
210 (458 ppm H_2O for KBH-2 vs. 319 ppm H_2O for HRV-147). This lower value for HRV-147 is
211 much more consistent with the amount (333 ppm H_2O) calculated using the ε_i from Koch-Müller
212 et al. (2007), as well as the lower concentrations in omphacites inferred by Katayama et al.
213 (2006) from their comparison of SIMS and FTIR data.

214 Due to the high variability in mean wavenumber among the clinopyroxenes in this study,
215 the overall correlation between H concentrations calculated using the Bell et al. (1995) vs.
216 Libowitzky and Rossman (1997) calibrations (Fig. 5) is weak ($r^2 = 0.89$), and especially poor if
217 just the diopside data are considered ($r^2 = 0.58$). However, the augites with self-similar spectra
218 follow a reasonable trend ($r^2 = 0.97$), with 20-30% lower concentrations calculated using the

219 latter calibration. This trend is also consistent with the measurements of Sundvall and Stalder
220 (2011) on augites from mantle xenoliths, while the data from Nazzareni et al. (2011) on Ca-rich
221 clinopyroxenes, dominated by low wavenumber absorption, are consistent with our data for
222 omphacite and some diopsides.

223 Some differences in calculated H_2O concentrations between our study (Table 1) and
224 previous work on the same samples should be noted. The largest discrepancies were found for
225 one diopside (95ADK1A) and two augites (ROM271-DI16 and KBH-2). Our newly selected
226 grain of 95ADK1A shows the same band structure as the crystal studied by Johnson et al. (2002)
227 – dominated by a single band centered at 3645 cm^{-1} – but has about 50% more H. The
228 discrepancy cannot be explained by any differences in baseline correction or crystal orientation,
229 but is instead likely related to the higher Fe^{3+} content of our crystal (Table 3); Johnson et al.
230 showed (in their Fig. 4a) that Fe^{3+} is correlated to the peak height at 3645 cm^{-1}. Furthermore, no
231 zoning was found in the cuboid we prepared, so the difference in H content appears to represent
232 grain-to-grain variation rather than zoning (although it is possible that a rim with different H
233 content was removed during polishing of the cuboid). For ROM271-DI16, we oriented a new
234 section to collect a new spectrum that was judged to be closer to β; consequently, the newly
235 derived H_2O content (472 ppm) is significantly higher than the value of 439 ppm H_2O given by
236 Bell et al. (2004), although within mutual estimated uncertainties. For KBH-2, we also measured
237 a higher H content (552 ppm H_2O) compared to the value (512 ppm H_2O) published by Bell and
238 Ihinger (2000). For this sample we oriented a new cuboid, after establishing a lack of zoning in
239 existing, polished slabs; we also oriented a second plate normal to the α and β directions to
240 double check our results. Finally, smaller discrepancies (4% or less) can be seen in Table 1 for
241 other samples studied previously at Caltech (PMR-53, ROM271-DI10, ROM271-DI21, HRV-

147, and LAC-236). For these samples we had to perform new baseline corrections in order to apply the Libowitzky and Rossman (1997) calibration, because the original corrected spectra (determined in most cases using a paper weighing method as described in Bell et al. 1995) were not available. We attempted to reproduce previously estimated peak heights (Bell et al. 1995; Bell, unpublished data; Smyth et al. 1991), but some loss of precision inevitably results from operator subjectivity in manually drawing baselines and/or differences in computer subtraction versus the paper weighing method.

SIMS

In Table 2 we list the average blank-corrected $^{16}O^{1}H/^{30}Si$, $^{16}O^{1}H/^{18}O$, and $^{19}F/^{30}Si$ ratios from three analyses of each sample (four in the case of PMR-53), as well as the average of the uncorrected values for the blank standard GRR510. In contrast to our work on olivine (Mosenfelder et al. 2011) and orthopyroxene (Mosenfelder and Rossman in press), we found no need to reject any analyses on the basis of Poisson counting statistics. Internal precision for $^{16}O^{1}H/^{30}Si$ ranged from 0.5 to 2% (2σ) for the natural clinopyroxenes containing H, and 5-7% (2σ) for the blank or "near blank" standards (GRR510 and ZM1cpxHT). Reproducibility was between 0.5 and 10% (2σ) for all natural clinopyroxenes except CIT17210; the poorer reproducibility (18%) for this relatively low-H sample may reflect a small degree of zoning that was not detected by FTIR. Internal precision was slightly better for $^{19}F/^{30}Si$, presumably due to higher count rates, ranging from 0.2 to 1% (2σ) for all samples except GRR510. Reproducibility was also better for $^{19}F/^{30}Si$, ranging from 1 to 5% (2σ).

The $^{16}O^{1}H$ SIMS data are plotted against H_2O concentrations determined using FTIR in Figure 6. Figures 6a and 6b show the results assuming the Bell et al. (1995) IR calibration (with

the value for PMR-53 fixed by manometry), with the data in Figure 6b normalized for SiO_2 content as determined by EPMA. Analogous plots are shown in Figures 6c and 6d for the Libowitkzy and Rossman (1997) IR calibration. The data were fit with both unweighted, ordinary least squares (OLS) regressions and York regressions (York 1966), which take into account uncorrelated errors on both SIMS data and FTIR/manometry data. A higher degree of data scatter is evident in Figure 6a/b compared to Figure 6c/d and consequently both types of fits are better for the frequency-dependent calibration of Libowitzky and Rossman; OLS fits have better correlation coefficients ($r^2 = 0.98$ vs. $r^2 = 0.92$, or $r^2 = 0.96$ vs. $r^2 = 0.93$ when normalized for SiO_2), while the York fits have lower mean standard weighted deviation (MSWD = 5 vs. 22). The OLS fit in Figure 6b also fails to intercept the origin and barely agrees with the York fit within its 95% confidence interval. Also shown in Figure 6b is the OLS fit for orthopyroxene using the Bell et al. (1995) calibration (Mosenfelder and Rossman in press); the datum for PMR-53 overlaps this line within uncertainty and the significance of this result is discussed further below. Finally, Figure 6c demonstrates that using either ^{30}Si or ^{18}O as the reference mass yields equivalent results, as we showed previously for orthopyroxene and olivine.

Fluorine concentrations (Table 2) were calculated from average $^{19}F/^{30}Si$ ratios multiplied by wt% SiO_2 (Table 3) using the two different calibration models outlined in Mosenfelder and Rossman (in press). F concentrations range from 17 to 458 ppm for model 1 and 8 to 214 ppm for model 2. For the rest of this paper we discuss only the model 2 values, which are referenced to more recent data (Guggino and Hervig 2011) on the basaltic glasses that we used for calibration. The highest measured concentrations are in two diopsides of crustal metamorphic origin (JLM77 and 95 ADK1A). Concentrations in the mantle clinopyroxenes are comparable to

concentrations measured for olivine and generally higher than concentrations measured in orthopyroxene (Mosenfelder and Rossman in press).

DISCUSSION

Accuracy of IR calibrations

Quantification of H concentrations in clinopyroxene using either FTIR or SIMS largely depends on two factors: the accuracy of IR calibrations based on measurements – in only a handful of samples – using quantitative techniques (Bell et al. 1995; Aubaud et al. 2009) and the applicability of these calibrations to samples with variable IR spectra. The latter issue was first raised by Bell et al. (1995) and further noted by Ingrin and Skogby (2000), who pointed out that the significantly lower mean wavenumber of IR spectra in many omphacites compared to other clinopyroxenes (as illustrated in Fig. 4) suggests that a frequency-dependent IR calibration should be used in preference to the single molar absorption coefficient measured by Bell et al. (1995). This conclusion is supported by subsequent FTIR-SIMS studies of omphacites (Katayama et al. 2006; Koch-Müller et al. 2007), as we discuss further below.

We begin our discussion of these two interrelated issues by comparing data for four samples (ROM271-DI10, PMR-53, ROM271-DI16, and ROM271-DI21) that have been used for SIMS calibration in three different laboratories (Aubaud et al. 2007; Wade et al. 2008; Tenner et al. 2009; this study). The last three of these samples were also studied directly by ERDA (Aubaud et al. 2009). Figure 7a shows excellent correlations between the SIMS calibrations conducted in the different laboratories, despite large differences in the measured ratios themselves. For the blank-corrected data of Tenner et al. (2009), the systematic shift in ratios compared to our data may result from differences in overall count rates, as discussed in

Mosenfelder et al. (2011), while variations in the data of Wade et al. (2008) may reflect variations in the value of the blank and/or calibration drift between sessions (we show only one of their three calibrations in Fig. 7a). The salient point of the graph is that the correlations shown imply that there is no significant heterogeneity among the nominally identical standards used by the different laboratories, which is important for the following discussion.

Figure 7b shows just our blank-corrected SIMS data for the above four samples, referenced to the three different FTIR calibrations used in this study. Note that for the Aubaud et al. (2009) calibration we plot the actual values determined directly by ERDA for the three samples they studied, rather than the significantly different values that would be calculated using their regressed molar absorption coefficient. This partially explains the relatively poor correlation coefficient ($r^2 = 0.84$) for a line regressed through that dataset. If their ε_i is used for all samples, the same correlation coefficient as for the Bell et al. calibration is obtained ($r^2 = 0.90$).

As with the full dataset shown in Figure 6, the highest correlation coefficient in Fig. 7b ($r^2 = 0.96$) is achieved by regressing the values calculated using the Libowitzky and Rossman (1997) calibration, implying that a frequency-dependent calibration better models the data. The same conclusion was reached for different reasons by Stalder and Ludwig (2007) for synthetic diopsides measured using FTIR and SIMS. In their case, the better fit of SIMS data to H concentrations calculated using the Libowitzky and Rossman (1997) calibration relies on the assumption that no matrix effect exists between pyroxenes and tourmalines, upon which their SIMS calibration was based.

As a thought exercise, if we were to eliminate ROM271-DI10 (which was not measured by ERDA) from Figure 7b, the regressions for all three calibrations would improve substantially.

333 However, the intercepts would be unrealistically high, considering that we have plotted blank
334 corrected data (with a well constrained, low H background as shown in the analytical methods
335 session). Note that this problem would not be mitigated if our 7% correction for the H content of
336 ROM271-DI16 (see the results section) was ignored and the original estimate of Bell et al.
337 (2004) used instead. The "problem sample" is in fact PMR-53, which plots at too low H content
338 and/or too high $^{16}O^{1}H/^{30}Si$ ratio relative to the other samples. This fact is disturbing as PMR-53
339 is the primary standard that was studied using multiple techniques. In the larger context, PMR-53
340 also agrees poorly with the best fits shown in Figures 6b and 6d for the full dataset. The relative
341 agreement among SIMS calibrations from multiple laboratories (Fig. 7a) suggests that sample
342 heterogeneity is not the cause of this behavior. We currently have no satisfactory answer to this
343 dilemma that has only been revealed by SIMS. One possibility to explain why PMR-53 is an
344 outlier on these plots is that there may be some systematic differences in baseline correction
345 among the samples. However, a significant underestimation of absorbance in the original
346 baseline correction for PMR-53 seems unlikely as that correction was informed from
347 examination of spectra from a dehydrated sample; we also note that in attempting to reproduce
348 that correction we not only duplicated the original value for total absorbance (to within one
349 A/cm) but also, apparently, the approximate shape of the curves, because our value calculated
350 using the Libowitzky and Rossman (1997) calibration is identical (within 1 ppm) to that given by
351 Aubaud et al. (2009).

352 A significant challenge for any H measurement using mass spectrometric, manometric, or
353 nuclear techniques is to reduce the level of the H background. For ERDA, the magnitude of the
354 background can be nearly comparable to the H content of the samples, which means that any
355 uncertainty in blank correction can led to large errors in the derived concentrations. Indeed,

Aubaud et al. (2009) concluded from analysis of multiple samples with low H contents that the level of their blank was variable, and therefore elected to subtract an average value of 102±81 ppm to correct their raw data. However, this large uncertainty in the blank cannot explain why the results for the Bell et al. calibration shown in Figure 7b mimic those of the Aubaud et al. calibration. Further analysis of these samples using a technique with low H background – that is not reliant on external calibration, as SIMS is – could solve this problem and also address the issue of a possible wavenumber dependence, because the calibrations that are currently available are all based on augites with relatively high mean wavenumber.

Revised frequency-dependent IR calibrations for clinopyroxene

There is no *a priori* reason to expect that the generic frequency-dependent IR calibration of Libowitzky and Rossman (1997) for hydrous minerals should be rigorously applicable for determining H in NAMs, even though theoretical studies (e.g., Balan et al. 2008) support the form of the frequency dependence (with molar absorption coefficients increasing linearly with decreasing wavenumber as the hydrogen bond length decreases). However, if we accept that a frequency-dependent calibration better fits the SIMS data, as argued above, a revised, provisional equation specific to clinopyroxene can be derived by redefining the parameters of their equation, which is simply a modification of the Beer-Lambert law:

$$\text{concentration (wt\% } H_2O) = A_i\,(\text{cm}^{-1}) \bullet 1.8/[t\,(\text{cm}) \bullet \rho(\text{g cm}^{-3}) \bullet \varepsilon_i\,(\text{L cm}^{-2}\ \text{mol}^{-1}\ H_2O)] \quad (1)$$

where A_i is integrated absorbance, 1.8 accounts for the molecular weight of H_2O, t is the path length (i.e., the sample thickness), ρ is the density of the mineral, and ε_i is the integral molar absorption coefficient, which takes the form

$$\varepsilon_i = a \bullet [\nu_0\text{-}\nu\ (\text{cm}^{-1})] \quad (2)$$

where ν is wavenumber and $a = 246.6$ and $\nu_0 = 3753$ are the parameters that were derived by Libowitzky and Rossman (1997). We fit our data by first assuming the H concentration of PMR-53 to be fixed either at the manometry value (268 ppm H_2O) or ERDA value (202 ppm H_2O). Next, we calculated values for other samples based on their $^{16}O^{1}H/^{30}Si$ x SiO_2 values, relative to PMR-53 (Table 2 and 3). We took into account the individually determined crystal densities and weighted the data according to uncertainties in total absorbance (Table 1). Then we fit the parameters a and ν_0 simultaneously to the absorbance data for all 13 H-bearing samples. This fitting exercise is similar to that performed by Stalder et al. (2012) on their SIMS and FTIR data on synthetic orthopyroxenes. Our best-fit values are

$a = 200$, $\nu_0 = 3805$ (assuming the manometry value for PMR-53) (3a)

$a = 266$, $\nu_0 = 3805$ (assuming the ERDA value for PMR-53) (3b)

Support for (3a) is given by the fact that the H concentration determined for HRV-147 (332 ppm H_2O) assuming the manometery value for PMR-53 is virtually identical to 333 ppm H_2O, the amount calculated using the ε_i from the SIMS-FTIR study of Koch-Müller et al. (2007). On the other hand, if the ERDA value for PMR-53 is used instead, HRV-147 is calculated to

have 250 ppm H_2O, similar to the value of 259 ppm H_2O calculated using the ε_i from Katayama et al. (2006). The accuracy of these calibrations remains to be verified. In the case of the study of Koch-Müller et al. (2007), as we noted previously (Mosenfelder et al. 2011), their SIMS calibration is tied to a suite of garnets analyzed with nuclear reaction analysis by Maldener et al. (2003), who derived an absorption coefficient for pyrope garnets much different than that measured by Bell et al. (1995) using manometry (and furthermore, their analysis ignores possible matrix effects between garnet and other phases). The Katayama et al. (2006) study may also suffer from similar assumptions with regards to a lack of matrix effects, as well as uncertainties propagated from using unpolarized spectra on unoriented samples. Nevertheless, both studies support the argument that a frequency-dependent IR calibration is needed for clinopyroxenes, particularly for omphacites and diopsides with lower mean wavenumber than augites.

It should be stressed that the uncertainties in equations (3a) and (3b) are large as they rely on the absolute H content of only one sample, and moreover that the validity of our fitting exercise rests on assumptions that will be difficult to evaluate until more "absolute" measurements on multiple samples are acquired. These assumptions include: 1) a correspondence between the uncertainties we estimated in the baseline for total absorbance (Table 1) and the uncertainties in baseline as a function of wavenumber, which are much more difficult to assess; 2) a lack of compositional effect on ε_i; 3) a linear dependence of ε_i on wavenumber; for olivine, defect-specific values for ε_i that vary in a non-linear way with wavenumber have also been proposed (Kovács et al. 2010; Balan et al. 2011); and 4) a lack of any intraphase matrix effects for SIMS (for instance due to differences in Fe content), which could explain some of the scatter in the SIMS data. We briefly discuss this last point at the end of the next section.

SIMS: matrix effects for H

Aubaud et al. (2007) addressed two types of matrix effects for SIMS analysis of H in NAMs, as we also discussed in Mosenfelder and Rossman (in press): interphase effects between different minerals, and intraphase effects due to differences in composition. The interphase effect is demonstrated in Figure 6b, where we compare our York regression for orthopyroxene (data collected during the same analytical session; slope = 0.0135) to that for clinopyroxene (slope = 0.0099), in both cases using the mineral-specific IR calibrations from Bell et al. (1995); the same comparison is shown in Figure 6d for the Libowitzky and Rossman (1997) calibration. The calibration for olivine (also collected during the same session) is not shown in Figure 6b but is in between the other fits, with a slope of 0.0104. Note that York and OLS regressions for each individual mineral yield nearly identical calibration slopes for orthopyroxene and olivine but not for clinopyroxene, betraying the higher level of uncertainty in the latter case.

Comparison of the fits in Figure 6b suggests that a significant matrix effect may exist between these phases, on the order of 35%. This difference is much less (only 15%) when the Libowitzky and Rossman (1997) calibration is assumed (Fig. 6d). Moreover, as previously noted, close examination of Figure 6b shows that PMR-53 falls within uncertainty on the line for orthopyroxene. Therefore, if the manometry data for both ortho- and clinopyroxene are correct there is no measurable matrix effect at all within mutual uncertainties. This conclusion would be roughly consistent with the calibrations shown by Tenner et al. (2009) on a smaller data set, although not with the different slopes shown by Aubaud et al. (2007) on the same samples. One possibility is that matrix effects may be more pronounced when $^{1}H^{-}$ is measured as opposed to $^{16}O^{1}H^{-}$. Furthermore, as discussed in Mosenfelder and Rossman (in press), the matrix effect

between orthopyroxene and olivine may also be unresolvable if the recent revision by Withers et al. (2012) of the IR absorption coefficient for olivine is correct.

Possible intraphase matrix effects are even more difficult to constrain than interphase effects but may partially explain the scatter in Figure 6. Our clinopyroxenes cover a wider range in composition than those used in other studies, and in any case the variations in major and minor element chemistry for clinopyroxene are larger than for olivines or orthopyroxenes that have been measured for hydrogen by SIMS (we have not been able to decipher any intraphase matrix effects for those two minerals). We looked for correlatives to relative ion yield by graphing $H_2O/(^{16}O^1H/^{30}Si \times SiO_2)$ against other chemical parameters (c.f., Hauri et al. 2002). Although we failed to find any robust correlations, one sample in particular suggests a possible matrix effect. KBH-2 contains much higher amounts of Al, Ca, and Ti (and lower Si) than the other augites and noticeably falls off the best fit trend when the data are normalized for SiO_2 in Figure 6d (even though it is well fit by the OLS regression in Fig. 6c). It is conceivable that the higher molar weight of this sample influences the yield of H and/or Si; the trend toward lower yield relative-to-Si that is seen Figure 6d would be consistent with previous work showing a negative correlation for hydrous glasses and minerals between molar weight of the matrix and H/Si ratios as measured by SIMS (King et al. 2002). Although intraphase matrix effects such as this may not be resolvable until uncertainties in FTIR data are addressed, they may become important when the hydrogen content of NAMs with significantly different major-element chemistry (e.g., Fe-rich pyroxenes or olivines in Martian rocks or experiments; Withers et al. 2011) are measured by SIMS.

Fluorine incorporation in clinopyroxene

Recent experimental work (Bernini et al. 2012; Beyer et al. 2012; Dalou et al. 2012) has shown that NAMs can contain surprisingly high amounts of F, up to hundreds or even thousands of ppm. For clinopyroxene, Dalou et al. (2012) measured as much as 626 ppm. Together with earlier studies in systems not deliberately doped with fluorine (Hauri et al. 2006; O'Leary et al. 2010), these results also demonstrate that F is more compatible than H in NAMs that are in equilibrium with melts or fluids. These experimental studies, as well as sparser measurements of F in natural NAMs (Hervig and Bell 2005; Guggino et al. 2007; Mosenfelder et al. 2011; Beyer et al. 2012), are beginning to refute the classic assumption (e.g., Smith et al. 1981) that F incorporation in NAMs can be ignored for the purpose of modeling the F budget of the Earth's crust and mantle (usually considered to be dominated by apatite, amphiboles, and micas). Although we measured much lower F concentrations in mantle clinopyroxenes compared to the maximum amounts measured in high P-T experiments, our results show that it is a ubiquitous trace element in this mineral, occurring at higher concentration levels (overall, or on average) compared to orthopyroxene (Mosenfelder and Rossman in press).

In Mosenfelder and Rossman (in press), we documented significantly lower F concentrations in orthopyroxenes and olivines derived from the crust compared to mantle samples, with one exception (a xenocryst from the Colorado Plateau with less than 1 ppm F). This situation is reversed for clinopyroxene, but this fact is not surprising given the geological context of the crustal diopsides we studied. 95ADK1A, containing the highest amount of F (214 ppm), comes from the Adirondacks (U.S.A.), in the same metamorphic terrane where Valley et al. (1983) documented high concentrations of F in grossular garnet (up to 7600 ppm). Likewise, we have measured (unpublished data) high F concentrations in V-rich grossulars from the Merelani Hills (Tanzania), the same locality as the V-rich diopsides CIT17210 (25 ppm F) and

JLM77 (90 ppm F). Furthermore, high F concentrations are seen in vanadian tremolites (0.5 wt%; Fritz et al. 2007) and phlogopites (up to 2 wt%; Giuliani 2008) from Merelani.

Fluorine concentrations in mantle-derived orthopyroxene and olivine from part I (Mosenfelder and Rossman in press) follow a systematic geographic trend, with distinctly lower amounts in xenocrysts from the Colorado Plateau (olivine and orthopyroxene both contain <1 ppm F) compared to samples from Kilbourne Hole (in the Rio Grande Rift, 7-9 ppm F) and South African kimberlites (6-47 ppm F in olivines, 12-17 ppm F in orthopyroxenes). Our clinopyroxene data, while limited, are in agreement with these results: BPcpxA, from the Colorado Plateau, contains the lowest amount of F we have measured in clinopyroxene (8 ppm), while samples from South Africa contain between 9 and 31 ppm. The highest concentration we measured in a mantle sample is in KBH-2 (47 ppm), which is a megacryst that may have been plucked from a different source (perhaps at higher pressure?) than the other samples we have measured from Kilbourne Hole (KBH-1 orthopyroxene and the ZM1 pyroxenes we dehydrated for use as potential blank standards). Again, all of these results are consistent with the simplistic notion put forth previously (Mosenfelder et al. 2011; Mosenfelder and Rossman in press) that different mantle reservoirs, particularly in sub-continental settings, have different amounts of F that are not necessarily correlated to H.

Whereas incorporation mechanisms for H in clinopyroxene have been explored extensively (e.g., Skogby and Rossman 1989; Smyth et al. 1991; Skogby 1994; Koch-Müller et al. 2004, 2007; Stalder and Ludwig 2007; Purwin et al. 2009; O'Leary et al. 2010), few constraints have been placed on modes of F incorporation. Because the ionic radius of F^- is close to that of OH^-, it is reasonable to assume that F substitutes into oxygen sites. One or more mechanisms are then needed for charge balance, such as:

$$^{IV}Al^{3+} + F^{-} \Leftrightarrow {}^{IV}Si^{4+} + O^{2-} \quad (4)$$

or

$$^{M2}Na^{+} + F^{-} \Leftrightarrow {}^{M2}Ca^{2+} + O^{2-} \quad (5)$$

(where IV and M2 refer to tetrahedral and M2 octahedral sites, respectively). Mechanisms involving vacancy formation or substitution of other cations in equations (4) and (5) can also be envisioned; for instance, Fe^{3+} in tetrahedral sites (Skogby 1994) or other monovalent cations (K^{+}, Li^{+}) in the M2 site could satisfy the charge balance. Equation (4) has been proposed as the primary mechanism for substitution of F in orthopyroxene (Beyer et al. 2012) and (by analogy) Cl in clinopyroxene (Dalou et al. 2012). However, the correlation between F and Al in orthopyroxene that was proposed by Beyer et al. (2012) was not seen by Dalou et al. (2012) or in Part I of this study (Mosenfelder and Rossman in press), countering this interpretation.

For clinopyroxene, Dalou et al. (2012) also found no correlation between F and Al, or any other major or minor element. The poor correlation between F and Al_2O_3 in their data is shown in Figure 8a, together with data from this study, which also show a lack of correlation when considered altogether. However, modest trends can be seen when our diopside and augite data are considered separately. Moreover, a strong correlation ($r^2 = 0.98$) is seen for diopsides when plotting only $^{IV}Al^{3+}$ against F (Fig. 8b), suggesting that equation (4) is especially important for F substitution in these samples. Note that the much more modest correlation ($r^2 = 0.70$) shown in Fig. 8b for augites goes away completely when the two samples from Kilbourne Hole (ZM1cpxHT and KBH-2, filled circles) that have higher $^{IV}Al^{3+}$ are taken out of the regression. The geographic sub-division that we delineate in this figure is relevant to the next part of the discussion.

537 The mechanism associated with equation (5) is explored in Figures 8c and 8d. When we
538 plot Na and K against F in Figure 8c, we once again find a lack of correlation when the samples
539 are considered altogether, although there is a modest correlation ($r^2 = 0.87$) just for the samples
540 from South Africa (five augites plus FRB-118, a mantle diopside). Furthermore, when we add
541 Figures 8b and 8c together (Na + K + ^{IV}Al plotted against F, Fig. 8d), a more robust correlation
542 ($r^2 = 0.92$) appears for all augites; note that omphacite and crustal-derived diopsides are left off
543 this plot, but two mantle-derived diopsides (FRB-118 and BPcpxA) plot close to the trend for
544 augites. This suggests that both mechanisms (4) and (5) are involved in F incorporation. This
545 inference is consistent with the inference by Dalou et al. (2012) from the shift of Raman
546 vibrational modes with increasing F content that F substitutes in the O3 site, which bridges both
547 tetrahedral and M2 cation sites.
548 The comparisons between major/minor element chemistry and trace F concentration
549 discussed above are subject to large uncertainties, due primarily to the uncertainties in
550 calculating cation proportions from EPMA data. For instance, we have poor constraints on the
551 oxidation state and site occupancies of Fe. Our calculation scheme in Table 3 fails to take into
552 account the possibility of Fe^{3+} in tetrahedral sites (because deficits in Si are preferentially filled
553 with Al), which could charge balance F by analogy with equation (4). This mechanism could be
554 relevant to 95ADK1A and KBH-2, which have the highest Si deficiencies and also high
555 Fe^{3+}/Fe_{Total}. Johnson et al. (2002) also assigned all Fe^{3+} in 95ADK1A to octahedral sites but
556 acknowledged that alternate interpretations of their Mössbauer spectra allowed for assignment of
557 some Fe^{3+} to tetrahedral sites, as seen in some synthetic samples (Skogby 1994).
558 Compared to H, the bonding environment of F is more difficult to study using
559 spectroscopic techniques. Studies of O-H vibrational frequencies using FTIR, while an indirect

probe of site occupancy, are highly sensitive to trace concentrations. The Raman shifts documented by Dalou et al. (2012) are not only an indirect probe (of F bonding to cations) but are very close to the limit of resolution. On the other hand, at higher concentration levels (in the weight percent range), both Raman and NMR (nuclear magnetic resonance) spectroscopies have been used successfully to investigate the solubility mechanisms of F in silicate glasses and melts (e.g., Mysen et al. 2004). By analogy with H incorporation mechanisms, for which much of our knowledge comes from doping studies – typically at higher concentrations than found in natural samples – we therefore suggest that future work to study the incorporation of F in NAMs should concentrate on samples synthesized at high P and T that contain higher amounts of F.

ACKNOWLEDGMENTS

Financial support for this research was provided by NSF grant EAR-0947956 to GRR, the Gordon and Betty Moore Foundation, and the White Rose Foundation. We thank Yunbin Guan, Chi Ma, and John Beckett for assistance with the ion microprobe, electron microprobe, and gas-mixing 1-atm furnace, respectively. We also thank Paul Asimow for discussions and assistance with some calculations; David Bell for kindly providing unpublished absorbance data for and continued use of samples he prepared while at Caltech; Elizabeth Johnson for discussion; Jennifer Wade for graciously providing data used in Figure 7; Zachary Morgan for the mineral separate used to make the ZM1cpxHT sample; and Monika Koch-Müller and Celia Dalou for reviews of the manuscript.

REFERENCES

582 Aubaud, C., Hauri, E.H., and Hirschmann, M.M. (2004) Hydrogen partitioning coefficients
583 between nominally anhydrous minerals and basaltic melts. Geophysical Research Letters,
584 31, doi: 10.1029/2004GL021341.
585 Aubaud, C., Withers, A.C., Hirschmann, M., Guan, Y., Leshin, L.A., Mackwell, S., and Bell,
586 D.R. (2007) Intercalibration of FTIR and SIMS for hydrogen measurements in glasses
587 and nominally anhydrous minerals. American Mineralogist, 92, 811-828.
588 Aubaud, C., Hirschmann, M.M., Withers, A.C., and Hervig, H.L. (2008) Hydrogen partitioning
589 between melt, clinopyroxene, and garnet at 3 GPa in a hydrous MORB with 6 wt.% H_2O.
590 Contributions to Mineralogy and Petrology, 156, 607-625.
591 Aubaud, C., Bureau, H., Raepsaet, C., Khodja, H., Withers, A.C., Hirschmann, M.M., and Bell,
592 D.R. (2009) Calibration of the infrared molar absorption coefficients for H in olivine,
593 clinopyroxene and rhyolitic glass by elastic recoil detection analysis. Chemical Geology,
594 262, 78-86.
595 Balan, E., Refson, K., Blanchard, M., Delattre, S., Lazzeri, M., Ingrin, J., Mauri, F., Wright, K.,
596 and Winkler, B. (2008) Theoretical infrared absorption coefficient of OH groups in
597 minerals. American Mineralogist, 93, 950-953.
598 Balan, E., Ingrin, J., Delattre, S., Kovács, I., and Blanchard, M. (2011) Theoretical infrared
599 spectrum of OH-defects in forsterite. European Journal of Mineralogy, 23, 295-292.
600 Bell, D.R. and Ihinger, P.D. (2000) The isotopic composition of hydrogen in nominally
601 anhydrous mantle minerals. Geochimica et Cosmochimica Acta, 64, 2109-2118.
602 Bell, D.R. and Rossman, G.R. (1992) Water in the Earth's mantle: the role of nominally
603 anhydrous minerals. Science, 255, 1391-1397.

604 Bell, D.R., Ihinger, P.D., and Rossman, G.R. (1995) Quantitative analysis of trace OH in garnet
605 and pyroxenes. American Mineralogist, 80, 465-474.
606 Bell, D.R., Rossman, G.R., Maldener, J., Endisch, D., and Rauch, F. (2003) Hydroxide in
607 olivine: a quantitative determination of the absolute amount and calibration of the IR
608 spectrum. Journal of Geophysical Research, 108(2105), DOI:10.1029/2001JB000679.
609 Bell, D.R., Rossman, G.R., and Moore, R.O. (2004) Abundance and partitioning of OH in a
610 high-pressure magmatic system: megacrysts from the Monastery Kimberlite, South
611 Africa. Journal of Petrology, 45, 1539-1564.
612 Bernini, D., Wiedenbeck, M., Dolejs, D., and Keppler, H. (2012) Partitioning of halogens
613 between mantle minerals and aqueous fluids: implications for the fluid flow regime in
614 subduction zones. Contributions to Mineralogy and Petrology, DOI:10.1007/s00410-012-
615 0799-4.
616 Beyer, C., Klemme, S., Wiedenbeck, M., Stracke, A., and Vollmer, C. (2012) Fluorine in
617 nominally fluorine-free mantle minerals: experimental partitioning of F between olivine,
618 orthopyroxene, and silicate melts with implications for magmatic processes. Earth and
619 Planetary Sciences, 337-338, 1-9.
620 Boyd, F.R., Dawson, J.B., and Smith, J.V. (1984) Granny Smith diopside megacrysts from the
621 kimberlites of the Kimberley area and Jagersfontein, South Africa. Geochimica et
622 Cosmochimica Acta, 48, 381-384.
623 Dalou, C., Koga, K.T., Shimizu, N., Boulon, J., and Devidal, J.L. (2012) Experimental
624 determination of F and Cl partitioning between lherzolite and basaltic melt. Contributions
625 to Mineralogy and Petrology, DOI 10.1007/s00410-011-0688-2.

626 Dowty, E. (1978) Absorption optics of low-symmetry crystals - application to titanian
627 clinopyroxene spectra. Physics and Chemistry of Minerals, 3, 173-181.
628 Droop (1986) A general equation for estimating Fe^{3+} concentrations in ferromagnesian silicates
629 and oxides from microprobe analyses, using stoichiometric criteria. Mineralogical
630 Magazine, 51, 431-435.
631 Fritz, E.A., Laurs, B.M., Downs, R.T., and Costin, G. (2007) Yellowish green diopside and
632 tremolite from Merelani, Tanzania. Gems and Gemology, 143, 146-148.
633 Grant, K.J., Ingrin, J., Lorand, J.P., and Dumas, P. (2007) Water partitioning between mantle
634 minerals from peridotite xenoliths. Contributions to Mineralogy and Petrology, 154, 15-
635 34.
636 Giuliani, G., Ohnenstetter, D., Palhol, F., Fenyrol, J., Boutroy, E., and de Boissezon, H., (2008)
637 Karelianite and vanadian phlogopite from the Merelani Hills gem zoisite deposits,
638 Tanzania. Canadian Mineralogist, 46, 1183-1194.
639 Guggino, S.N. and Hervig, R.L. (2011) Synthesis and characterization of five new F-bearing
640 basalt reference materials (Fba glasses): quantifying the fluorine content of the basaltic
641 glass standards BCR-2G, BHVO-2G, GSA-1G, GSC-1G, GSD-1G, GSE-1G, ML3B-G,
642 KL2-G, and ALV-519-4. American Geophysical Union, Fall Meeting 2011, abstract
643 #V31C-2535.
644 Guggino. S.N., Hervig, R.L., and Bell, D.R. (2007) Fluorine in olivine from plutonic, extrusive,
645 and hypabbysal suites. American Geophysical Union, Fall Meeting 2007, abstract
646 #V41B-0609.
647 Gunter, M.E. (2004) The polarized light microscope: should we teach the use of a 19th century
648 instrument in the 21st century? Journal of Geoscience Education, 52, 34-44.

649 Hauri, E.H., Wang, J., Dixon, J.E.,, King, P.L., Mandeville, C., and Newman, S. (2002) SIMS
650 analysis of volatiles in silicate glasses 1. Calibration, matrix effects and comparisons with
651 FTIR. Chemical Geology, 183, 99-114.
652 Hauri, E.H., Gaetani, G.A., and Green, T.H. (2006) Partitioning of water during melting of the
653 Earth's upper mantle at H_2O-undersaturated conditions. Earth and Planetary Science
654 Letters, 248, 715-734.
655 Hervig, R.L. and Bell, D.R. (2005) Fluorine and hydrogen in mantle megacrysts. American
656 Geophysical Union, Fall Meeting 2005, abstract #V41A-1426.
657 Ingrin, J. and Skogby, H. (2000) Hydrogen in nominally anhydrous upper-mantle minerals:
658 concentration levels and implications. European Journal of Mineralogy, 12, 543-570.
659 Ito, J. (1975) High temperature solvent growth of orthoenstatite, $MgSiO_3$, in air. Geophysical
660 Research Letters, 2, 533-536.
661 Johnson, E.A., Rossman, G.R., Dyar, M.D., and Valley, J.W. (2002) Correlation between OH
662 concentration and oxygen isotope diffusion rate in diopsides from the Adirondack
663 Mountains, New York. American Mineralogist, 87, 899-908.
664 Katayama, I., Nakashima, S., and Yurimoto, H. (2006) Water content in natural eclogite and
665 implication for water transport into the deep upper mantle. Lithos, 86, 245-259.
666 King, P.L., Venneman, T.W., Holloway, J.R., Hervig, R.L., Lowenstern, J.B., and Forneris, J.F.
667 (2002) Analytical techniques for volatiles: a case study using intermediate (andesitic)
668 glasses. American Mineralogist, 87, 1077-1089.
669 Koch-Müller, M., Matsyuk, S.S., and Wirth, R. (2004) Hydroxyl in omphacites and omphacitic
670 clinopyroxenes of upper mantle to lower crustal origin beneath the Siberian platform.
671 American Mineralogist, 89, 921-931.

672 Koch-Müller, M., Matsyuk, S.S., Rhede, D., Wirth, R., and Khisina, N. (2006) Hydroxyl in
673 mantle olivine xenocrysts from the Udachnaya kimberlite pipe. Physics and Chemistry of
674 Minerals, 33, 276-287.
675 Koch-Müller, M., Abs-Wurmbach, I., Rhede, D., Kahlenberg, V., and Matsyuk, S. (2007)
676 Dehydration experiments on natural omphacites: qualitative and quantitative
677 characterization by various spectroscopic methods. Physics and Chemistry of Minerals,
678 34, 663-678.
679 Koch-Müller, M. and Rhede, D. (2010) IR absorption coefficients for water in nominally
680 anhydrous high-pressure minerals. American Mineralogist, 95, 770-775.
681 Kovács, I., Hermann, J., O'Neill, H.S.C., Fitz Gerald, J., Sambridge, M., and Horváth, G. (2008)
682 Quantitative absorbance spectroscopy with unpolarized light: Part II. Experimental
683 evaluation and development of a protocol for quantitative analysis of mineral spectra.
684 American Mineralogist, 93, 765-778.
685 Kovács, I., O'Neill, H.S.C., Hermann, J., and Hauri, E.H. (2010) Site-specific infrared O-H
686 absorption coefficients for water substitution into olivine. American Mineralogist, 95,
687 292-299.
688 Li, Z.-X., Lee, C.-T., Peslier, A.H., Lenardic, A., and Mackwell, S.J. (2008) Water contents in
689 mantle xenoliths from the Colorado Plateau and vicinity: implications for the mantle
690 rheology and hydration-induced thinning of continental lithosphere. Journal of
691 Geophysical Research, 113, B09210, doi:10.1029/2007JB005540.
692 Libowitzky, E. and Rossman, G.R. (1997) An IR absorption calibration for water in minerals.
693 American Mineralogist, 82, 1111-1115.

694 Maldener, J., Hösch, A., Langer, K., and Rauch, F. (2003) Hydrogen in some natural garnets
695 studied by nuclear reaction analysis and vibrational spectroscopy. Physics and Chemistry
696 of Minerals, 30, 337-344.
697 McCormick, T. C. (1986) Crystal-chemical aspects of nonstoichiometric pyroxenes. American
698 Mineralogist, 71, 1434-1440.
699 Mosenfelder, J.L. and Rossman, G.R. (in press) Analysis of hydrogen and fluorine in pyroxenes:
700 part I. Orthopyroxene. American Mineralogist.
701 Mosenfelder, J.L., Le Voyer, M., Rossman, G.R., Guan, Y., Bell, D.R., Asimow, P.D., and Eiler,
702 J.M. (2011) Analysis of hydrogen in olivine by SIMS: evaluation of standards and
703 protocol. American Mineralogist, 96, 1725-1741.
704 Mysen, B.O., Cody, G.D., and Smith, A. (2004) Solubility mechanisms of fluorine in peralkaline
705 and meta-aluminous silicate glasses and in melts to magmatic temperatures. Geochimica
706 et Cosmochimica Acta, 68, 2745-2769.
707 Nazzareni, S., Skogby, H., and Zanazzi, P.F. (2011) Hydrogen content in clinopyroxene
708 phenocrysts from Salina mafic lavas (Aeolian arc, Italy). Contributions to Mineralogy
709 and Petrology, 162, 275-288.
710 O'Leary, J.A., Rossman, G.R., and Eiler, J.M. (2007) Hydrogen analysis in minerals by
711 continous-flow mass spectrometry. American Mineralogist, 92, 1990-1997.
712 O'Leary, J.A., Gaetani, G.A., and Hauri, E.H. (2010) The effect of tetrahedral Al^{3+} on the
713 partitioning of water between clinopyroxene and silicate melt. Earth and Planetary
714 Science Letters, doi:10.1016/j.epsl.2010.06.011.
715 Paterson, M.S. (1982) The determination of hydroxyl by infrared absorption in quartz, silicate
716 glasses, and similar materials. Bulletin de Minéralogie, 105, 20-29.

717 Peslier, A.H., Luhr, J.F., and Post, J. (2002) Low water content in pyroxenes from spinel-
718 peridotites of the oxidized, sub-arc mantle wedge. Earth and Planetary Science Letters,
719 201, 69-86.
720 Purwin, H., Stalder, R., and Skogby, H. (2009) Hydrogen incorporation in Fe- and Na-doped
721 diopsides. European Journal of Mineralogy, 21, 691-704.
722 Roden, M.F. and Smith, D. (1979) Field geology, chemistry, and petrology of Buell Park minette
723 diatreme, Apache County, Arizona. In F.R. Boyd and H.O.A. Meyer, Eds., Kimberlites,
724 Diatremes, and Diamonds: Their Geology, Petrology, and Geochemistry, p. 364-381.
725 American Geophysical Union, Washington, D.C.
726 Shannon, R.D., Dickinson, J.E., and Rossman, G.R. (1992) Dielectric constants of crystalline
727 and amorphous spodumene, anorthite and diopside and the oxide additivity rule. Physics
728 and Chemistry of Minerals, 19, 148-156.
729 Skogby, H. (1994) OH incorporation in synthetic clinopyroxene. American Mineralogist, 79,
730 240-249.
731 Skogby, H. and Rossman, G.R. (1989) OH- in pyroxene: an experimental study of incorporation
732 mechanisms and stability. American Mineralogist, 74, 1059-1069.
733 Skogby, H. and Rossman, G.R. (1991) The intensity of amphibole OH bands in the infrared
734 absorption spectrum. Physics and Chemistry of Minerals, 18, 64-68.
735 Skogby, H., Bell, D.R., and Rossman, G.R. (1990) Hydroxide in pyroxene: variations in the
736 natural environment. American Mineralogist, 75, 764-774.
737 Smith, J.V., Delaney, J.S., Hervig, R.L., and Dawson, J.B. (1981) Storage of F and Cl in the
738 upper mantle: geochemical implications. Lithos, 14, 133- 147.

739 Smyth, J.R., Bell, D.R., and Rossman, G.R. (1991) Incorporation of hydroxyl in upper-mantle
740 clinopyroxenes. Nature, 351, 732-735.
741 Stalder, R. and Ludwig, T. (2007) OH incorporation in synthetic diopside. European Journal of
742 Mineralogy, 19, 373-380.
743 Stalder, R., Prechtel, R., and Ludwig, T.L. (2012) No site-specific infrared absorption
744 coefficients for OH-defects in pure enstatite. European Journal of Mineralogy, 24, 465-
745 470.
746 Sundvall, R. and Stalder, R. (2011) Water in upper mantle pyroxene megacrysts and xenocrysts:
747 a survey study. American Mineralogist, 96, 1215-1227.
748 Tenner, T.J., Hirschmann, M.M., Withers, A.C., and Hervig, R.L. (2009) Hydrogen partitioning
749 between nominally anhydrous upper mantle minerals and melt between 3 and 5 GPa.
750 Chemical Geology, 262, 42-56.
751 Valley, J.W., Essene, E.J., and Peacor, D.R. (1983) Fluorine-bearing garnets in Adirondack calc-
752 silicates. American Mineralogist, 68, 444-448.
753 Wade, J.A., Plank, T., Hauri, E.H., Kelley, K.A., Roggensack, K., and Zimmer, M. (2008)
754 Prediction of magmatic water contents via measurement of H_2O in clinopyroxene
755 phenocrysts. Geology, 36, 799-802.
756 Withers, A.C. (in press) On the use of unpolarized infrared spectroscopy for quantitative analysis
757 of absorbing species in birefringent crystals. American Mineralogist.
758 Withers, A.C., Hirschmann, M.M., and Tenner, T.J. (2011) The effect of Fe on olivine H_2O
759 storage capacity: consequences for H_2O in the martian mantle. American Mineralogist,
760 96, 1039-1053.

761 Withers, A.C., Bureau, H., and Raepsaet, C., and Hirschmann, M.M. (2012) Calibration of
762 infrared spectroscopy by elastic recoil detection analysis of H in synthetic olivine.
763 Chemical Geology, 334, 92-98.
764 York, D. (1966) Least-squares aitting of a straight line. Canadian Journal of Physics. 44, 1079-
765 1086.

766

767
768
769 **Tables**

770 **Table 1.** FTIR data

771 **Table 2.** SIMS data

772 **Table 3.** EPMA data

773 **Appendices**

774 **Appendix 1.** FTIR spectra of clinopyroxenes, including baselines.

775 **Appendix 2.** SIMS analyses of clinopyroxene, April 2012

776

777 **Figure captions**

778

779 **Figure 1.** Polarized IR spectra in the first silicate overtone region for clinopyroxenes. Diopside
780 and augite are represented by spectra for 62047-70B and PMR-53, respectively; both samples
781 were well oriented. Spectra for all diopsides closely resemble those of 62047-70B. Most augites
782 resemble PMR-53, but some intermediate compositions show patterns intermediate between
783 diopside and augite; an example is shown using partial spectra for ROM271-10 in α and β (for
784 this sample, absorbance was too high in this region for γ and at lower wavenumbers than shown

for α and β). All spectra normalized to 1 cm, presented without baseline correction, and offset for clarity.

Figure 2. Polarized IR spectra of diopsides in the α, β, and γ orientations. Sample numbers are labeled directly above each spectrum. All spectra normalized to 1 cm, shown without baseline correction, and offset for clarity.

Figure 3. Polarized IR spectra of augites in the α, β, and γ orientations. Sample numbers are labeled directly above each spectrum. All spectra normalized to 1 cm, shown without baseline correction, and offset for clarity.

Figure 4. Polarized spectra of HRV-147 omphacite compared to KBH-2 augite. Sample numbers and polarization directions are labeled above each spectrum. All spectra normalized to 1 cm, shown without baseline correction, and offset for clarity.

Figure 5. Comparison of H concentrations determined using the calibrations of Bell et al. (1995) and Libowitzky and Rossman (1997). Open symbols are our data for augites (circles), diopsides (squares) and omphacite (triangle). Smaller, filled symbols are data from Nazzareni et al. (2011)(squares) and Sundvall and Stalder (2011)(circles). Regression line ($r^2 = 0.97$) shown only for our data on augites (spectra shown in Fig. 3). Regressions through diopside data alone or through our complete dataset show worse correlation coefficients ($r^2 = 0.58$ and $r^2 = 0.89$, respectively). Regressions through datasets of Nazzareni et al. and Sundvall and Stalder give $r^2 = 0.96$ and $r^2 = 0.95$, respectively.

808

809 **Figure 6.** SIMS versus FTIR data for hydrogen. SIMS data are blank corrected, with error bars
810 ($2\sigma_{SD}$) shown. Error bars for FTIR data are discussed in the text. **a.** Bell et al. (1995) IR
811 calibration assumed; line shows ordinary least squares (OLS) fit. **b.** Same data as in **a**,
812 normalized for SiO_2 content as measured by EPMA. Grey line is a York regression, with 95%
813 confidence intervals shown as dashed lines; the lower confidence interval shown nearly
814 coincides with the OLS fit (solid black line). The black dashed line is our SIMS calibration
815 (York regression) for orthopyroxene, also using the Bell et al. (1995) IR calibration; datum for
816 PMR-53 overlaps this line within uncertainty. **c.** Libowitzky and Rossman (1997) IR calibration
817 assumed. Data are shown for both ^{30}Si (open black circles) and ^{18}O (filled grey circles) as the
818 reference mass, yielding essentially identical correlation coefficients for the OLS fits as shown. **d.**
819 Same data as in **c**, normalized for SiO_2 content. In this case, OLS and York regressions are
820 nearly coincident. York regression for orthopyroxene is also shown (black dashed line).

821

822 **Figure 7. a.** Inter-laboratory comparison of SIMS data for four samples (ROM271-DI10, PMR-
823 53, ROM271-DI16, and ROM271-DI21). Our results are compared against selected data from
824 the CIW and ASU SIMS labs, from Wade et al. (2008) and Tenner et al. (2009), respectively. **b.**
825 Data for the same four samples references to the three IR calibrations used in this study; values
826 (Table 1) determined directly by ERDA (Aubaud et al. 2009) or manometry (Bell et al. 1995) are
827 plotted where applicable. Labeled samples are discussed in text.

828

829 **Figure 8.** F contents as a function of major and minor element abundance in clinopyroxenes. All
830 F data from this study plotted using model 2 values. **a.** Alumina versus F. Data from this study

are compared to analyses from six experiments by Dalou et al. (2012). **b.** Tetrahedral Al versus F for our data only. Separate regressions shown for diopsides ($r^2 = 0.98$) and augites ($r^2 = 0.70$; both filled and open circles); datum for omphacite was not included in any regression. **c.** Na and K versus F. The regression shown ($r^2 = 0.87$) includes five augites and one diopside from South Africa. **d.** Na + K + ^{IV}Al versus F. Here the regression shown ($r^2 = 0.92$) is for all augites. A regression through just the South African samples as in Figure 8c would give a different slope and higher correlation coefficient ($r^2 = 0.95$).

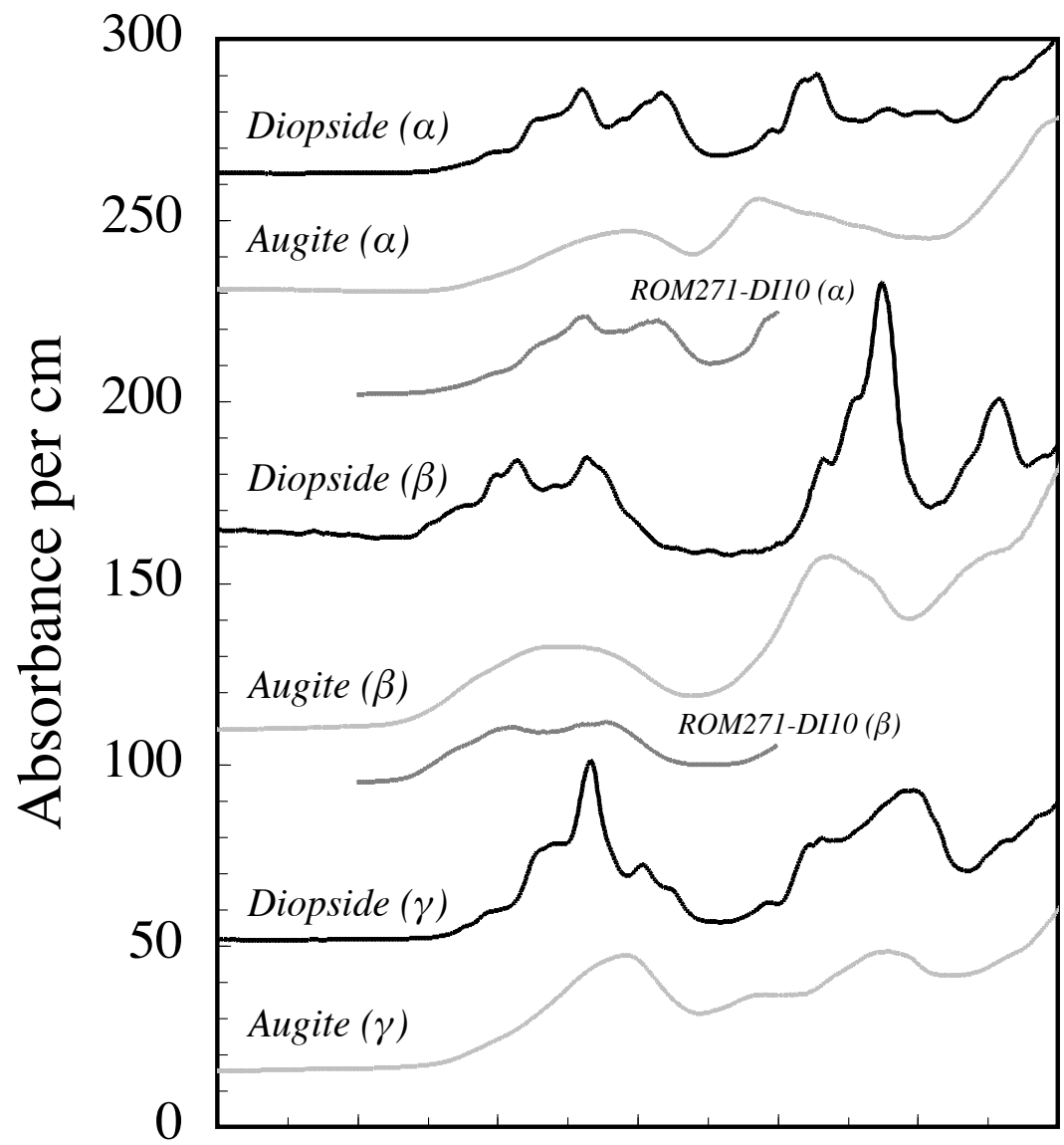

Mosenfelder et al., Fig. 1

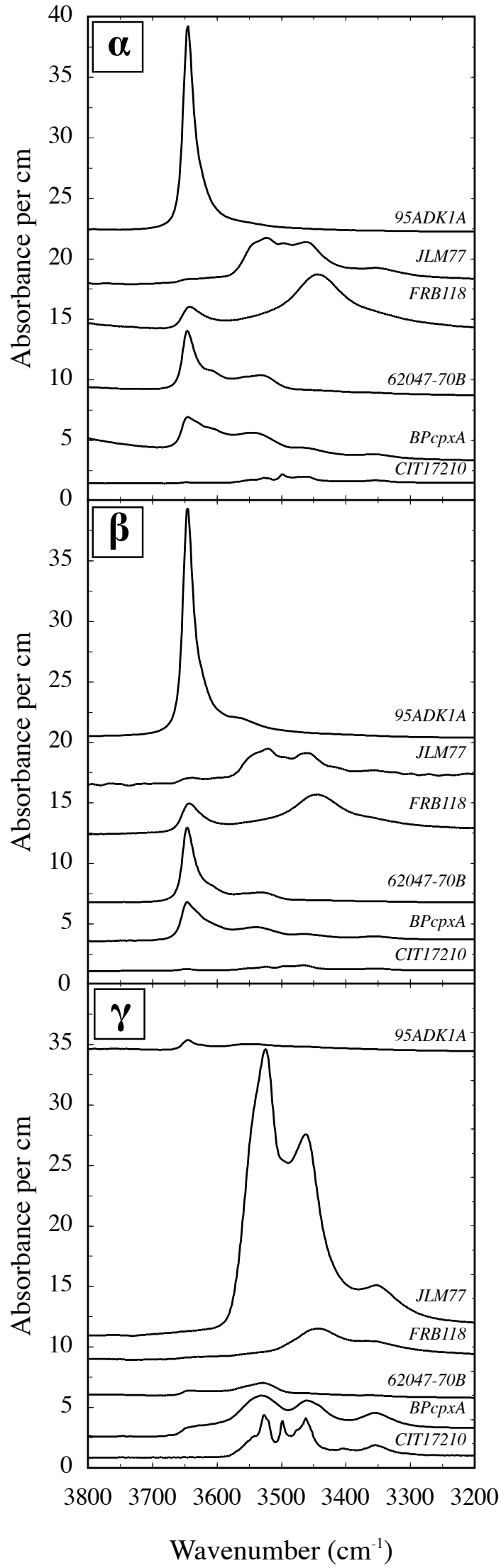

Mosenfelder et al., Fig. 2

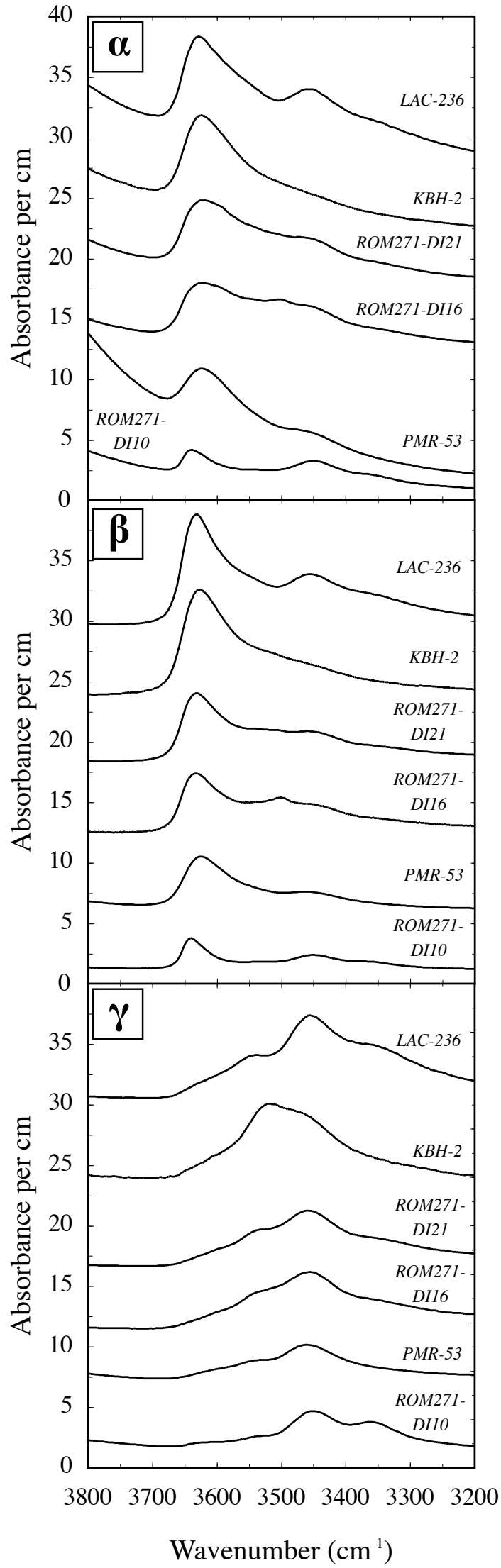

Mosenfelder et al., Fig. 3

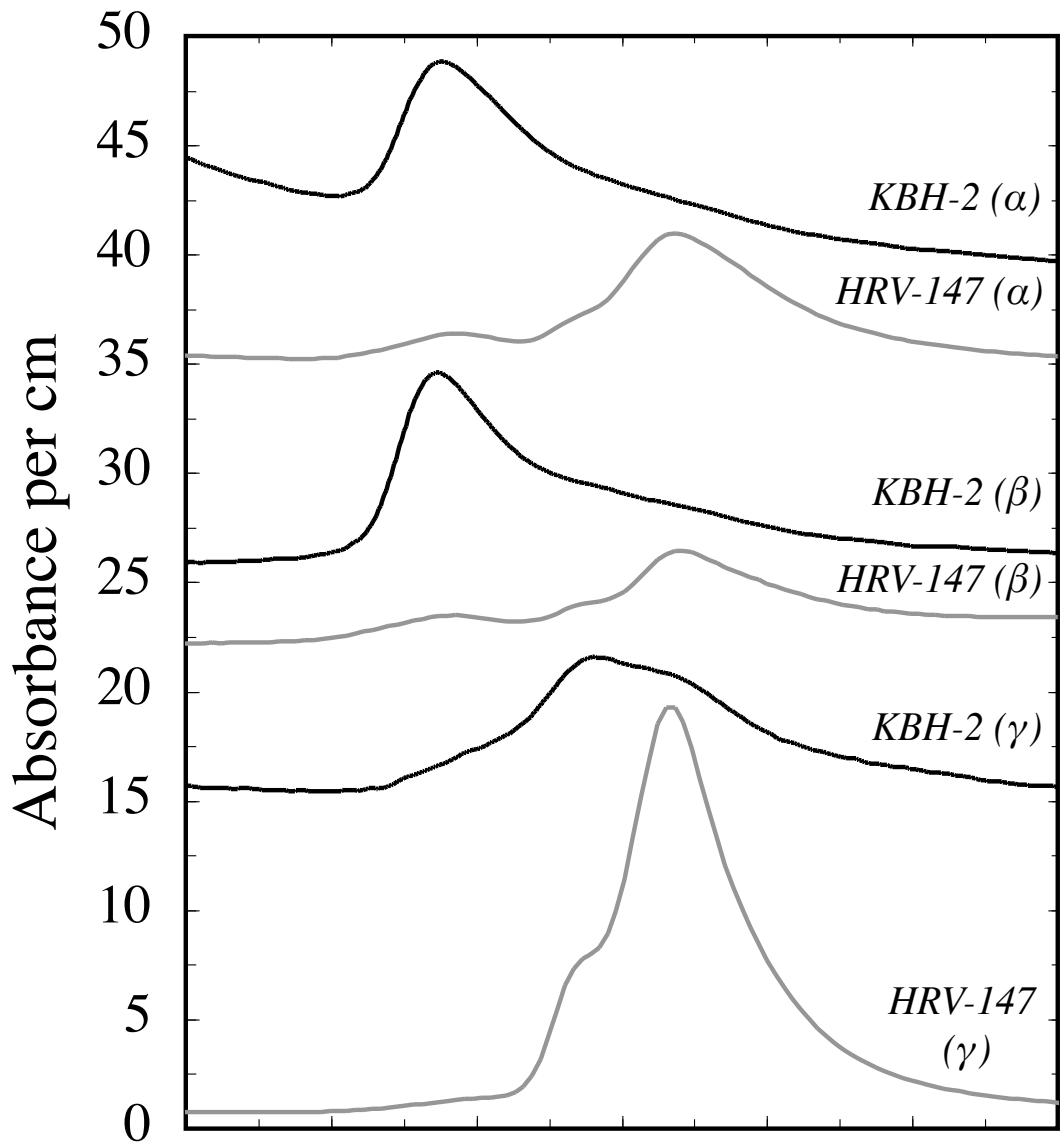

Mosenfelder et al., Fig. 4

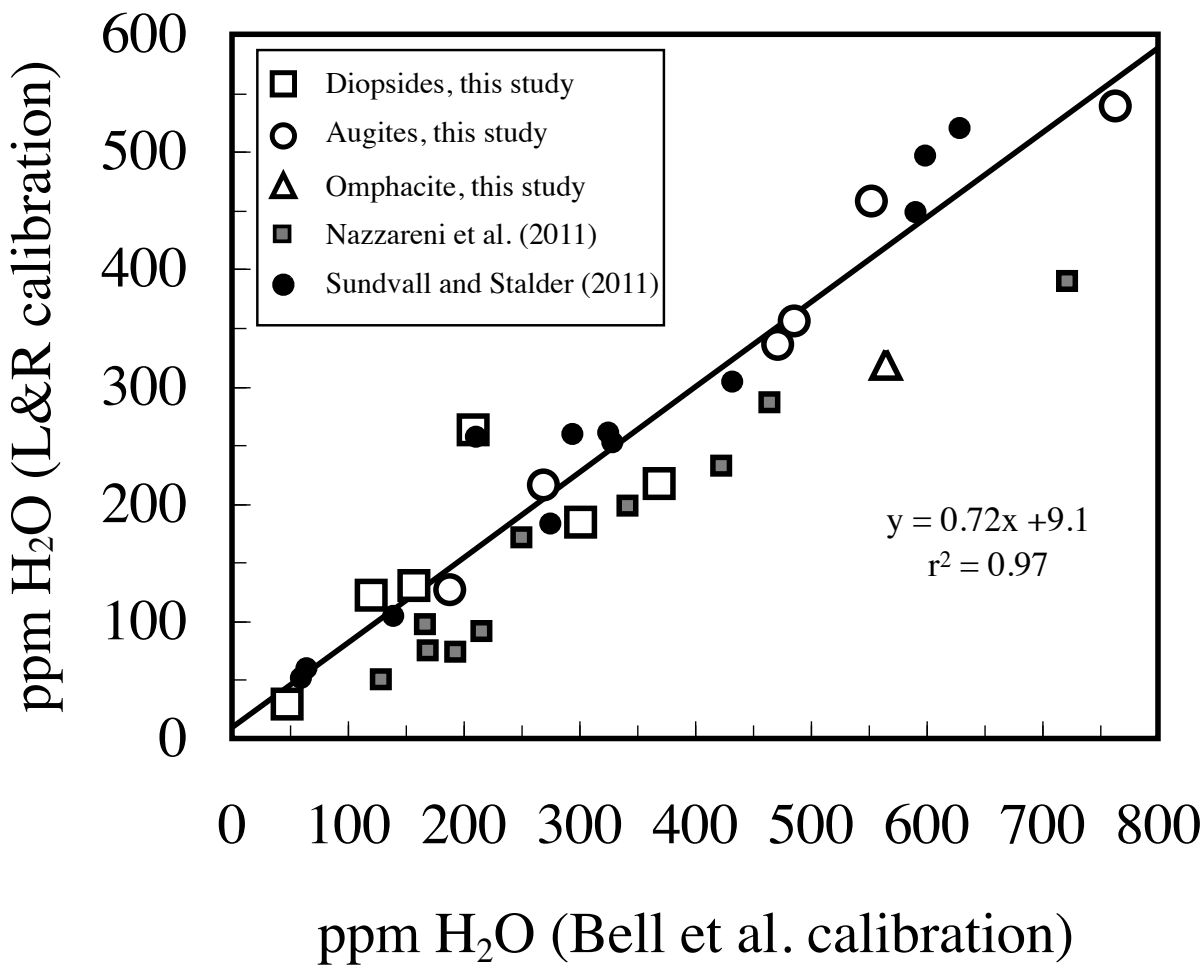

Mosenfelder et al., Fig. 5

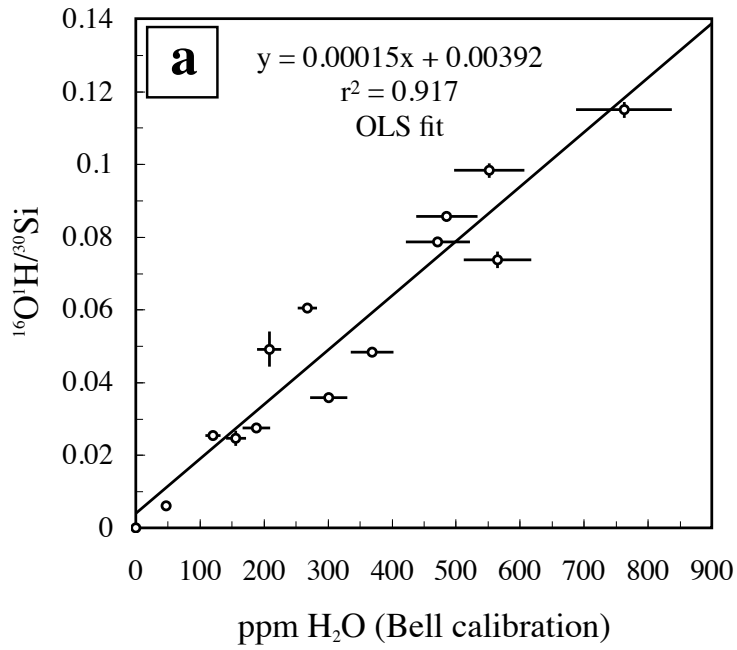

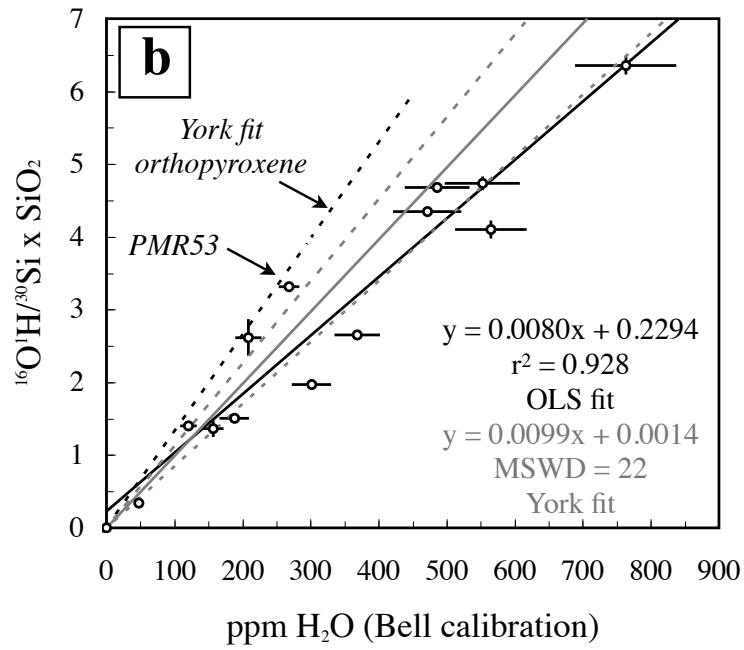

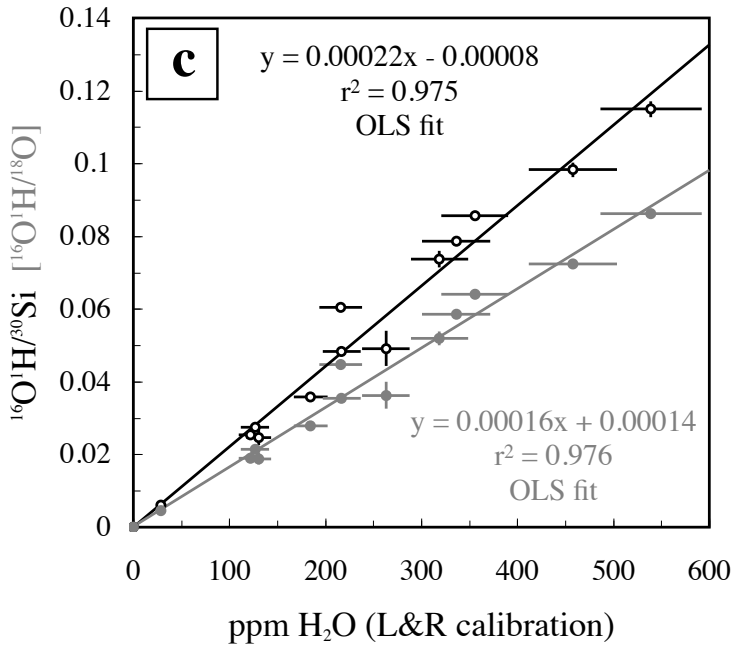

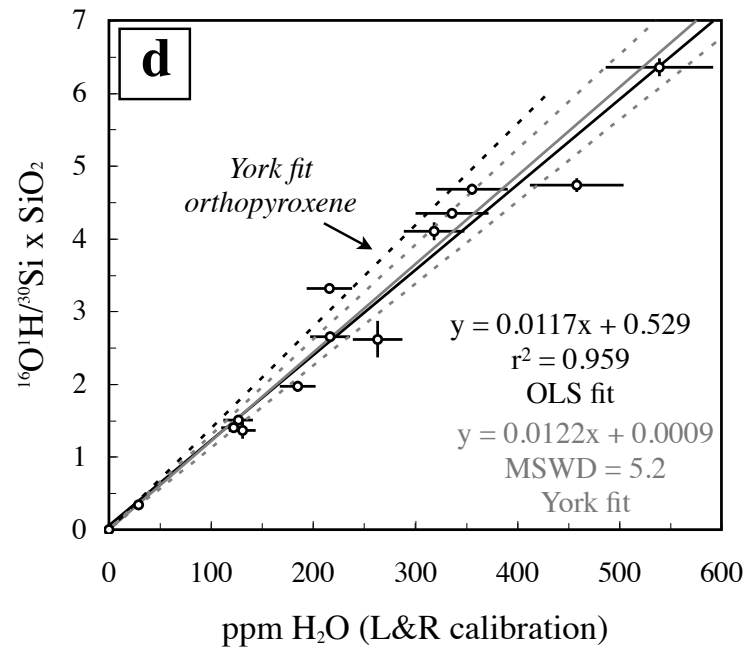

Mosenfelder et al., Fig. 6

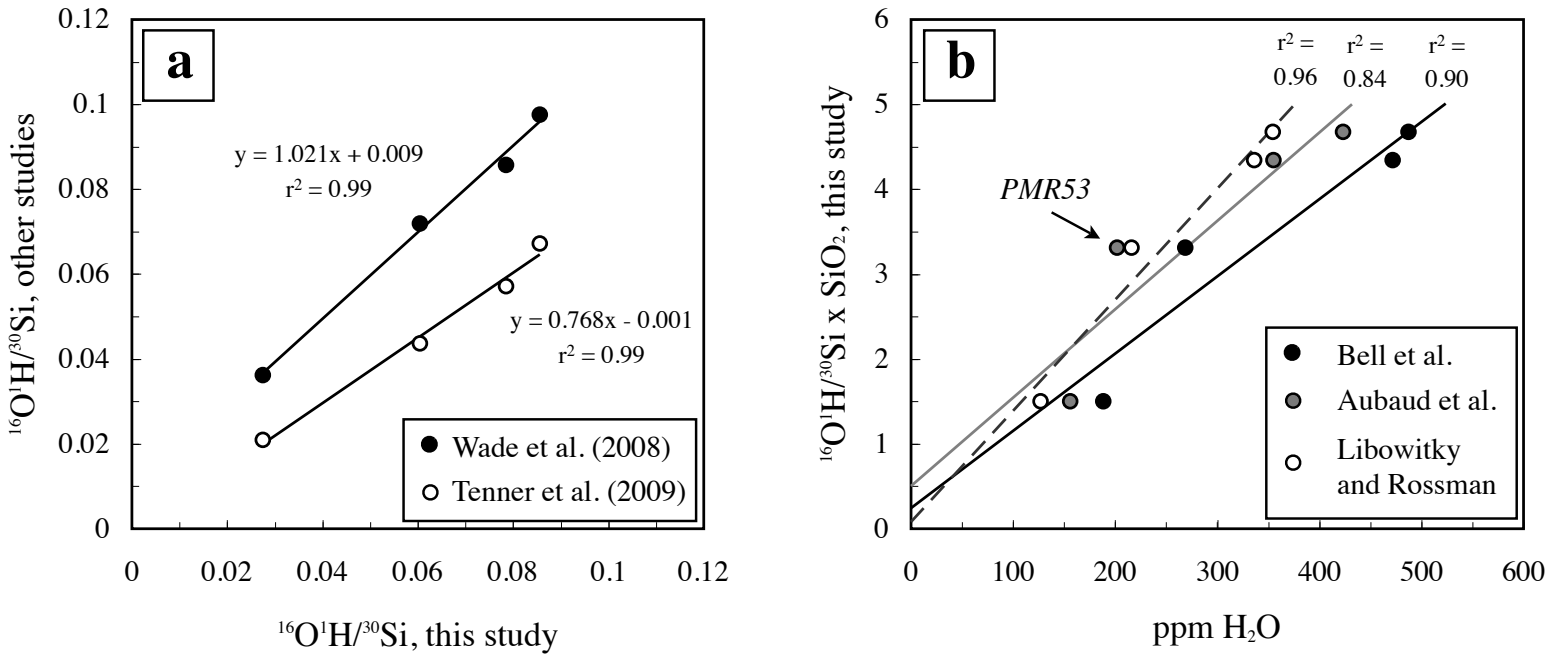

Mosenfelder et al., Fig. 7

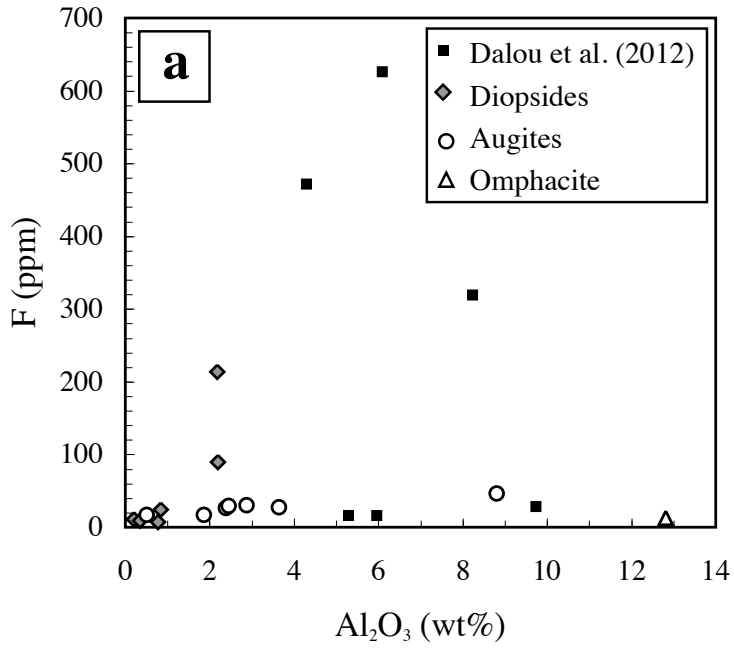

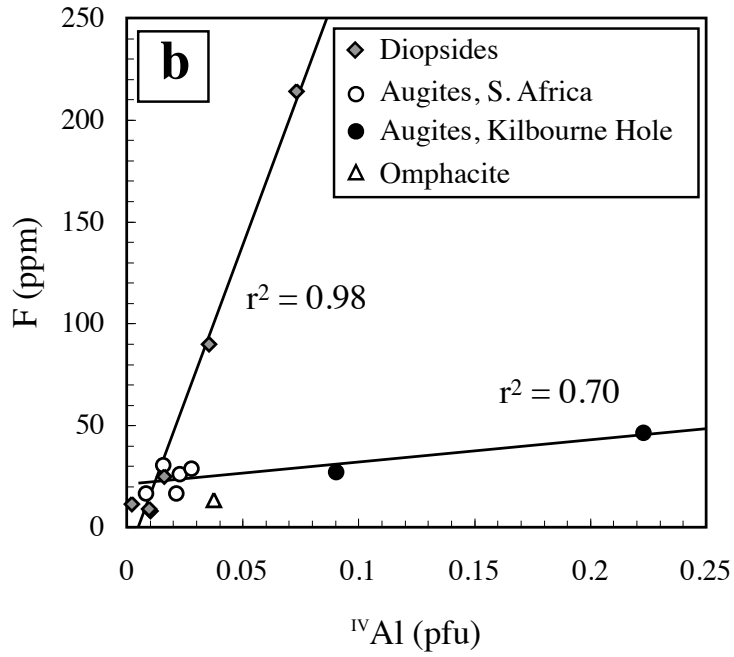

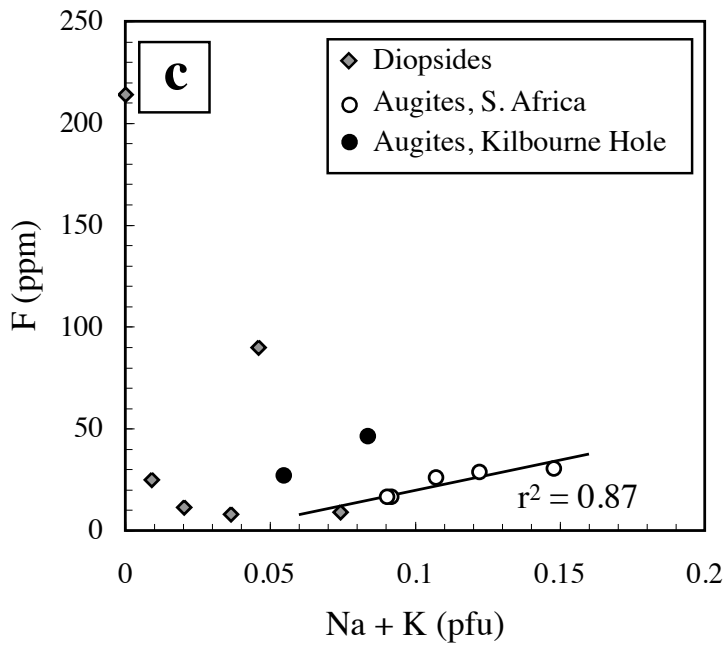

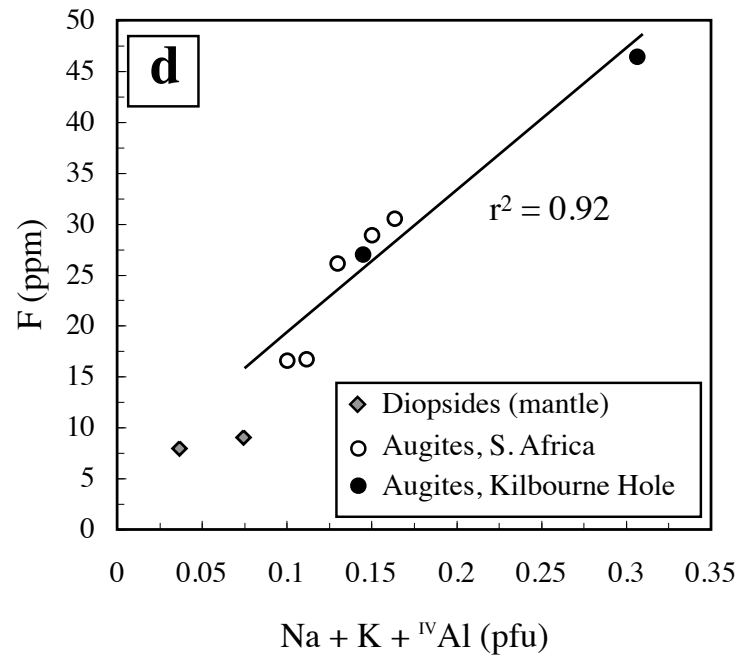

Mosenfelder et al., Fig. 8

Table 1. FTIR data

Sample no.	Locality	Density *	IR integrated absorbance/cm				H_2O, Bell	H_2O, Aubaud	H_2O, L&R	References
		Mg/m^3 (2s)	a	b	g	A (total)	(ppmw)	(ppmw)	(ppmw)	
GRR510	Synthetic	–	0	0	0	0	0	0	0	Ito (1975); Skogby et al. (1990)
ZM1cpxHT	Kilbourne Hole, New Mexico, U.S.A. (dehydrated)	–	0	0	0	0	0	0	0	This study
CIT17210	Merelani Hills, Tanzania	3.273(5)	78(2)	71(11)	182(9)	331(14)	48(5)	39(5)	29(3)	Fritz et al. (2007)****
BPcpxA	Buell Park, Arizona, U.S.A.	3.295	443(40)	328(26)	327(20)	1098(52)	157(16)	130(16)	131(13)	Roden and Smith (1979)***
62047-70B	Russia	3.295(3)	370(33)	304(9)	171(17)	846(39)	121(12)	100(12)	122(12)	Shannon et al. (1992)
ROM271-DI10	Monastery Mine, S. Africa	3.339	542(81)	382(27)	412(45)	1336(97)	188(22)	156(21)	127(15)	Bell et al. (2004)
FRB118	Jagersfontein Mine, S. Africa	3.295	913(55)	704(42)	496(25)	2114(74)	302(29)	250(30)	185(18)	Boyd et al. (1984)****
JLM77	Merelani Hills, Tanzania	3.277(7)	731(22)	438(22)	1403(28)	2572(42)	369(33)	306(36)	217(20)	Fritz et al. (2007)****
95ADK1A	Adirondack Mountains, New York, U.S.A.	3.295	577(29)	756(23)	128(13)	1461(39)	208(19)	173(20)	263(24)	Johnson et al. (2002)
PMR-53	Premier Mine, S. Africa	3.339(17)	577	630	697	1904	268(15)**	202(28)***	216(22)	Skogby et al. (1990); Bell et al. (1995)
HRV-147	Roberts Victor Mine, S. Africa	3.340	1060(106)	690(35)	2264(23)	4014(114)	565(53)	469(56)	319(30)	Skogby et al. (1990); Smyth et al. (1991); Bell and Rossman
ROM271-DI16	Monastery Mine, S. Africa	3.339	1178(153)	1072(107)	1102(55)	3351(195)	472(50)	355(41)***	336(36)	Bell et al. (2004)
ROM271-DI21	Monastery Mine, S. Africa	3.339	1203(96)	1132(68)	1118(89)	3453(148)	486(48)	423(70)***	356(35)	Bell et al. (2004)
KBH-2	Kilbourne Hole, New Mexico, U.S.A.	3.361(7)	1117(145)	1437(72)	1397(84)	3950(182)	552(55)	459(57)	458(46)	Bell and Ihinger (2000)
LAC-236	Lace Mine, S. Africa	3.339	1788(179)	1887(94)	1746(87)	5421(220)	763(75)	634(77)	539(53)	This study

"Bell", "Aubaud", and "L&R" refer to IR calibrations by Bell et al. (1995), Aubaud et al. (2009), and Libowitzky and Rossman (1997), respectively
Uncertainties in absorbance measurements and H_2O concentrations are discussed in text
*2s uncertainty given for samples large enough to make density measurements; see text for assumptions about other samples
**Value and uncertainy for PMR-53 are from manometry measurements of Bell et al. (1995); uncertainty for L&R calibration assumed to be 10%
***Values and uncertainties determined by ERDA (Aubaud et al. 2009)
****Reference cited for general locality information, not specific sample

Table 2: SIMS data

Sample No.	$^{16}O^{1}H/^{30}Si$	$^{16}O^{1}H/^{18}O$	$^{19}F/^{30}Si$	Fluorine (ppm) *	
				Model 1	Model 2
GRR510	*0.0004(3)*	*0.0003(2)*	*0.0008(3)*	0	0
ZM1cpxHT	0.0006(1)	0.00073(4)	0.1334(62)	57(3)	27(1)
CIT17210	0.0061(11)	0.0045(7)	0.1217(62)	55(3)	25(1)
BPcpxA	0.0247(21)	0.0188(16)	0.0386(13)	17.4(8)	8.0(3)
62047-70B	0.0253(2)	0.0190(3)	0.0555(19)	25(1)	11.6(4)
ROM271-DI10	0.0275(5)	0.0214(1)	0.0805(12)	35.7(8)	16.6(2)
FRB118	0.0358(14)	0.0278(9)	0.0439(6)	19.7(5)	9.1(1)
JLM77	0.0483(12)	0.0354(4)	0.4369(142)	194(7)	90(3)
95ADK1A	0.0492(48)	0.0363(36)	1.0654(416)	458(18)	214(8)
PMR53	0.0604(3)	0.0447(7)	0.1475(32)	66(2)	30.5(7)
HRV147	0.0738(23)	0.0519(19)	0.0653(9)	29.5(6)	13.7(2)
ROM271-DI16	0.0786(3)	0.0585(4)	0.1251(12)	56.0(8)	26.1(3)
ROM271-DI21	0.0856(14)	0.0640(13)	0.1404(14)	62.1(9)	28.9(3)
KBH-2	0.0982(20)	0.0724(9)	0.2553(38)	99(2)	46.4(7)
LAC-236	0.1149(22)	0.0861(10)	0.0803(28)	36(2)	16.7(6)

All values blank corrected except for values in italics for GRR510

Uncertainties (in parentheses) are $2s_{SD}$ from the average of three analyses for each sample (or four each for GRR510 and PMR53)

* models 1 and 2 described in Mosenfelder and Rossman (in revision); uncertainties in F content do not take into account uncertainties in calibı

ration

Table 3. EPMA data

Sample no.	GRR510	ZM1cpxHT	CIT17210	BPcpxA	62047-70B	ROM271-DI10	FRB-118	JLM77	95ADK1A	PMR-53	HRV-147	ROM271-DI16	ROM271-DI21	KBH-2	LAC-236
SiO_2	51.93(25)	52.91(19)	55.52(16)	55.18(8)	55.53(13)	54.67(7)	55.14(28)	54.88(10)	53.28(17)	54.89(9)	55.61(19)	55.30(19)	54.67(11)	48.22(12)	55.30(11)
TiO_2	–	0.17(1)	–	0.04(1)	–	0.15(1)	0.17(2)	0.12(2)	0.12(1)	0.35(1)	0.29(1)	0.338(4)	0.48(2)	1.34(1)	0.13(2)
Al_2O_3	–	3.65(5)	0.83(2)	0.77(2)	0.19(2)	0.50(1)	0.34(2)	2.19(1)	2.17(6)	2.88(2)	12.80(8)	2.39(1)	2.45(2)	8.81(3)	1.87(3)
VO_2*	3.41(3)														
V_2O_3*	–	0.04(1)	0.028(3)	0.038(3)	–	0.05(1)	0.037(3)	0.61(1)	–	0.04(1)	0.02(1)	0.03(2)	0.043(4)	0.06(1)	0.03(1)
Cr_2O_3	–	1.15(4)	–	0.48(1)	0.54(2)	0.30(2)	1.30(3)	–	–	0.16(1)	0.08(2)	0.30(2)	0.18(1)	–	0.44(2)
FeO	–	2.68(2)	0.09(3)	2.16(2)	1.06(2)	5.25(7)	2.00(4)	–	1.89(3)	7.06(4)	2.12(3)	5.47(6)	6.11(7)	6.75(4)	4.02(3)
MnO	–	–	0.26(1)	0.05(1)	–	0.10(2)	0.06(1)	0.08(2)	0.06(1)	0.15(1)	–	0.12(1)	0.13(1)	0.14(1)	0.11(1)
MgO	17.27(16)	17.00(6)	18.00(4)	17.01(3)	17.78(8)	15.87(3)	17.22(6)	17.33(8)	16.68(4)	18.12(6)	8.65(9)	20.32(6)	18.53(3)	13.62(4)	19.95(11)
CaO	25.22(7)	21.88(8)	26.17(12)	24.43(8)	25.23(12)	21.93(3)	22.99(6)	24.74(10)	26.30(11)	13.78(6)	13.17(3)	14.18(6)	15.43(11)	19.17(8)	16.90(9)
Na_2O	0.12(2)	0.78(3)	0.13(3)	0.52(1)	0.29(2)	1.30(1)	1.06(5)	0.59(3)	–	2.09(2)	6.13(9)	1.53(1)	1.73(3)	1.17(3)	1.24(5)
K_2O	0.52(3)	–	–	–	–	–	–	–	–	0.030(3)	0.26(1)	0.026(5)	0.027(3)	–	0.094(3)
NiO	–	–	–	–	–	–	–	–	–	0.06(4)	0.11(1)	0.10(2)	0.04(4)	–	–
Total	98.47	100.26	101.03	100.68	100.62	100.12	100.33	100.54	100.50	99.61	99.24	100.10	99.82	99.28	100.08
Tetrahedral positions															
Si	1.9222	1.9097	1.9839	1.9899	1.9981	1.9916	1.9905	1.9647	1.9269	1.9842	1.9625	1.9772	1.9720	1.7771	1.9785
Al	–	0.0903	0.0161	0.0101	0.0019	0.0084	0.0095	0.0353	0.0731	0.0158	0.0375	0.0228	0.0280	0.2229	0.0215
V^{4+}*	0.0778	–	–	–	–	–	–	–		–	–	–	–	–	–
Octahedral positions															
Al	–	0.0650	0.0188	0.0227	0.0061	0.0131	0.0049	0.0571	0.0194	0.1069	0.4949	0.0779	0.0762	0.1598	0.0574
Ti	–	0.0046	–	0.0011	–	0.0041	0.0046	0.0032	0.0033	0.0095	0.0077	0.0091	0.0130	0.0371	0.0035
V^{3+}	0.0136	0.0012	0.0008	0.0011	–	0.0015	0.0011	0.0175	–	0.0012	0.0006	0.0009	0.0012	0.0018	0.0009
Cr	–	0.0328	–	0.0137	0.0154	0.0086	0.0371	–	–	0.0046	0.0022	0.0085	0.0051	–	0.0124
Fe^{3+}**	–	0.0366	0.0027	0.0068	0.0007	0.0688	0.0314	–	0.0472	0.0320	0.0001	0.0246	0.0416	0.0706	0.0341
Fe^{2+}	–	0.0443	0.0000	0.0583	0.0312	0.0911	0.0290	–	0.0099	0.1815	0.0624	0.1390	0.1427	0.1374	0.0862
Mn	–	–	0.0079	0.0015	–	0.0031	0.0018	0.0024	0.0018	0.0046	–	0.0036	0.0040	0.0044	0.0033
Mg	0.9530	0.9147	0.9588	0.9145	0.9537	0.8619	0.9267	0.9249	0.8993	0.9765	0.4551	1.0831	0.9964	0.7483	1.0641
Ca	1.0002	0.8462	1.0019	0.9440	0.9727	0.8560	0.8892	0.9490	1.0191	0.5337	0.4980	0.5432	0.5963	0.7570	0.6478
Na	0.0086	0.0546	0.0090	0.0364	0.0202	0.0918	0.0742	0.0458	–	0.1465	0.4641	0.1061	0.1210	0.0836	0.0860
K	0.0246	–	–	–	–	–	–	–	–	0.0014	0.0117	0.0012	0.0012	–	0.0043
Ni	–	–	–	–	–	–	–	–	–	0.0017	0.0031	0.0029	0.0012	–	–

Notes: structural formulae determined by normalizing to four cations. Numbers in parentheses represent one standard deviation of results from five analyses per sample
Dashes represent elements under the detection limit; P was also analyzed but below detection limit in all samples
*Valence state of V assumed to be predominantly 4+ in GRR510 only; see text for discussion.
** Fe^{3+} calculated using the method of Droop (1986).